A co-conserved gene pair supports *Caulobacter* iron homeostasis during chelation stress

Sergio Hernandez Ortiz[1], Kiwon Ok[1,2], Thomas V. O'Halloran[1,2,3], Aretha Fiebig[1,*], Sean Crosson[1,*]
[1]Department of Microbiology, Genetics & Immunology, Michigan State University, East Lansing, MI, USA
[2]Elemental Health Institute, Michigan State University, East Lansing, MI, USA
[3]Department of Chemistry, Michigan State University, East Lansing, MI, USA
*Correspondence should be addressed to A.F. or S.C. (fiebigar@msu.edu; crosson4@msu.edu)

Synthetic metal chelators are widely used in industrial, clinical, and agricultural settings, leading to their accumulation in the environment. Although the effects of chelators on metal solubility and bioavailability are well documented, their impact on microbial physiology is not well defined. We measured the growth of *Caulobacter crescentus*, a common soil and aquatic bacterium, in the presence of the ubiquitous chelator ethylenediaminetetraacetic acid (EDTA) and found that it restricts growth by reducing intracellular iron levels. Using barcoded transposon sequencing, we identified an operonic gene pair, *cciT–cciO*, that is required to maintain iron homeostasis during EDTA challenge. *cciT* encodes one of four TonB-dependent transporters that are regulated by the ferric uptake repressor (Fur) and stands out among this group of genes in its ability to support *Caulobacter* growth across diverse media conditions. The function of CciT strictly requires *cciO*, which encodes a cytoplasmic Fe^{II} dioxygenase-family protein. Our results thus define a functional partnership between an outer membrane iron receptor and a cytoplasmic dioxygenase that are broadly co-conserved in Proteobacteria. We expanded our analysis of the *cciT–cciO* system to natural environments by measuring the growth of mutant strains in freshwater from two ecologically distinct lakes, which have significantly different nutritional and geochemical profiles compared to standard laboratory media. *cciT* and *cciO* were not required for growth in lake water, regardless of EDTA presence, highlighting the iron acquisition versatility of *Caulobacter* in *bona fide* environments and underscoring the conditional toxicity of EDTA. This study defines a conserved iron acquisition system and bridges laboratory-based physiology studies to real-world environments.

Introduction

Microbes are central to the productivity of aquatic and terrestrial ecosystems (1), playing a key role in the biogeochemical cycling of elements and the degradation of complex organic biopolymers into assimilable molecules (2). However, anthropogenic chemicals can perturb microbial physiology and community structure (3, 4) and affect ecological balance (5–9). The broad-spectrum metal chelator ethylenediaminetetraacetic acid (EDTA) is widely used in industrial applications (10) and in personal, medical, and food products (11, 12). Global production of EDTA and related synthetic chelators reaches hundreds of thousands of tons per year (13, 14). These chelators have been detected in the environment at varying concentrations and pose a potential threat to ecosystem health because they bind essential metal ions (10, 15), which can broadly perturb microbial physiology (16–18). Studies of microbial genes that influence fitness under chelation stress are needed as we work to understand the effects of these ubiquitous molecules on microbial biology.

Caulobacter species provide excellent models for such studies, as they are ecologically (19) and metabolically (20–24) versatile and prevalent in both soil and aquatic ecosystems (19). These gram-negative bacteria have important roles in soils, where they are reported to enhance the growth of model plant systems (25, 26) and have been identified as ecological hub species in plant-associated microbial communities in the rhizosphere and phyllosphere (27, 28). Here we report a randomly barcoded transposon sequencing approach (RB-TnSeq) (29) to identify genes that contribute to *Caulobacter crescentus* fitness in a complex medium containing a growth-limiting concentration (300 μM) of EDTA. This approach led to the discovery of genes whose disruption diminished or enhanced bacterial fitness during EDTA challenge. Genes directly controlled by several metal-responsive regulators, including the ferric uptake repressor (Fur) (30, 31), the zinc uptake repressor (Zur) (32), and a uranium/zinc/copper-responsive two-component system (UzcRS/CusRS) (33, 34), were among those that influence fitness in the presence of EDTA. However, a subset of genes in the Fur regulon were identified as major fitness determinants at the tested growth-limiting EDTA concentration.

We focused specifically on a functional analysis of two genes that are directly regulated by Fur, are co-conserved and syntenic across Proteobacteria, and strongly support *C. crescentus* fitness in EDTA-containing media: *cciT*, encoding a TonB-dependent outer membrane transporter, and *cciO*, encoding an uncharacterized 2-oxoglutarate (2OG) Fe^{II}-dependent dioxygenase. CciT is related to the Fiu transporter of *E. coli* and the PiuA transporters of select gram-negative pathogens including *Acinetobacter baumannii*, *Burkholderia pseudomallei*, and *Pseudomonas aeruginosa*. Fiu and PiuA transporters import Fe^{III}-catecholate siderophores, including the catecholate antibiotic cefiderocol (FDC) (35–38). Like *cciT*, *fiu* and *piuA* are typically adjacent to a 2OG/Fe^{II}-dependent dioxygenase gene on the chromosome. To our

knowledge, a functional connection between these syntenic genes has remained undefined to date.

In this study, we demonstrate that EDTA treatment results in decreased intracellular iron levels in *C. crescentus* and that the *cciT* and *cciO* genes are critical for growth under chelation stress. Through a systematic genetic analysis of Fur-regulated outer membrane transport systems, we show that the function of CciT has a strict – and specific – requirement for CciO. Our data thus demonstrate a central role for these two proteins in maintenance of iron homeostasis in the presence of a high-affinity chelator. Our study illuminates the versatility of *C. crescentus* iron-acquisition mechanisms in physicochemically-complex systems, advances understanding of the genetic foundations of bacterial resilience under chelation stress, and defines the functional role of a broadly co-conserved pair of iron homeostasis genes in this context.

Results

Genetic contributors to *Caulobacter* fitness under EDTA chelation stress

To identify *Caulobacter* genes that affect fitness in the presence of EDTA, we implemented a randomly barcoded transposon (Tn) sequencing approach (RB-TnSeq) (29) using a previously described *C. crescentus Tn*-Himar mutant library (39, 40). We separately cultivated the library in liquid peptone-yeast extract (PYE) medium and in liquid PYE medium containing 300 μM EDTA. This concentration enabled the identification of genes with relative positive and negative effects on fitness in the presence of EDTA when they are disrupted, as it resulted in a 50% decrease in growth of the wild-type strain (Figure S1). The relative fitness of most mutant strains was unaffected by EDTA treatment (Figure 1A). Mutant strains with the lowest fitness scores in medium containing EDTA included those with defects in cell envelope and cell development functions (mutation of CCNA_01118, *bamE*, *fabZ*, *divJ*) or with predicted nutrient acquisition functions (mutation of CCNA_00028 and CCNA_03155-03159) (Figure 1A and Table S1). Mutants of the polar cell development regulator gene *divJ* (41) were among a group of several strains with fitness defects regardless of the presence or absence of EDTA in the medium (Table S1). While mutation of CCNA_01118, *bamE*, or *fabZ* led to basal fitness defects in untreated liquid medium, EDTA treatment exacerbated these defects. The CCNA_01118 gene is located adjacent to *divJ* and *fssA* (42), suggesting that it has a role in polar cell development. *fabZ* is part of a genetic locus with important functions in lipopolysaccharide and outer membrane biogenesis (43), while *bamE* encodes a component of the β-barrel protein assembly machine complex in *Caulobacter* (44). The EDTA sensitivity phenotype of *bamE* insertional mutants is consistent with a previous report (45).

CCNA_00028 encodes a putative TonB-dependent transporter (TBDT) which belongs to a class of outer membrane proteins that function in the acquisition of vitamin B_{12}, ferric siderophore complexes, nickel complexes, and carbohydrates (46). Disrupting *CCNA_00028* had no effect on fitness in liquid medium without EDTA but led to lower fitness in the presence of EDTA. In fact, mutants of *CCNA_00028* had the most severe fitness defects in EDTA, relative to

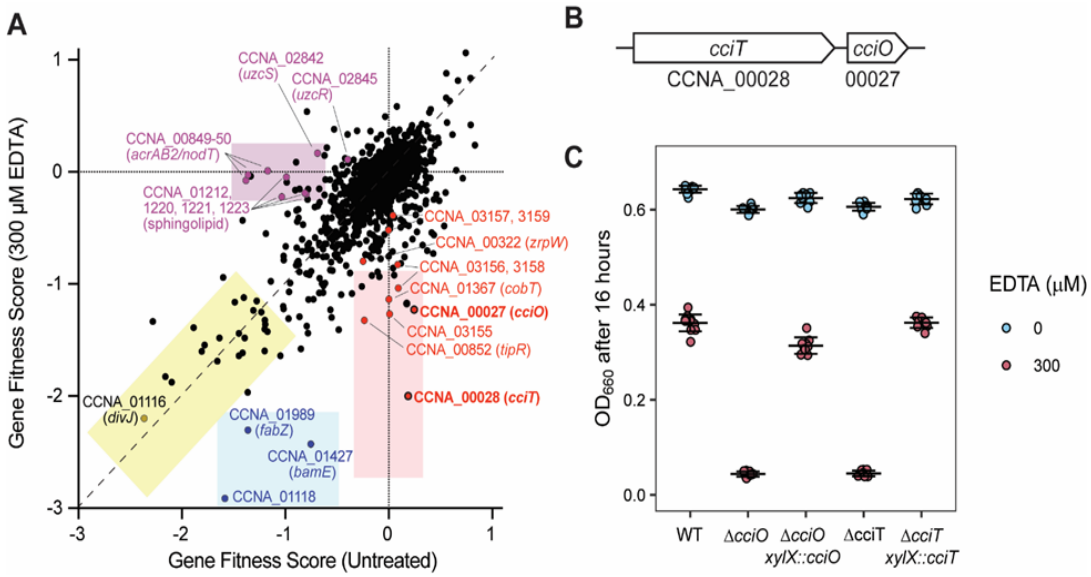

Figure 1. Identification of genes that contribute to *C. crescentus* fitness in the presence of EDTA. (A) Fitness scores of *C. crescentus* genes after cultivation of a barcoded Tn-himar mutant library in complex PYE medium (Untreated) or in the same medium containing 300 μM EDTA for 16 h. Each point represents one gene. Scores represent the average of four independent cultures in each condition. Multiple classes of fitness defects are observed: the yellow box highlights genes that lead to similar growth defects when disrupted regardless of EDTA; the blue box shows genes that have a fitness defect in PYE medium when disrupted that is more severe in the presence of EDTA; the pink box highlights genes that have a fitness defect when disrupted specifically in PYE medium containing EDTA; the purple box highlights genes that have a basal fitness defect in PYE medium that is rescued by the addition of EDTA. Representative genes for each class are shown. The complete fitness data set is presented in Table S1. **(B)** Diagram of the *cciT–cciO* locus. **(C)** Optical density of the wild-type (WT) strain and strains bearing in-frame deletions of *cciO* (Δ*cciO*) or *cciT* (Δ*cciT*), and deletion strains expressing the gene from its native promoter from an ectopic insertion site after 16 h of growth in liquid PYE medium alone (blue) or containing 300 μM EDTA (red). All cultures were inoculated at a starting optical density (OD_{660}) of 0.01. Box plots reflecting the median and the 25th and 75th percentiles are overlaid with the individual data points for each independent culture (WT, n = 24; Δ*cciO* and Δ*cciT*, n = 18; complementation strains, n = 6).

untreated medium, in the entire dataset (Table S1). Other mutants with large relative defects in the presence of EDTA included mutants in the directly adjacent gene *CCNA_00027,* encoding a likely 2OG/Fe^{II}-dependent dioxygenase (Figure 1B), and in CCNA_03155–03159, encoding a PepSY-like system implicated in periplasmic reduction of ferric iron and iron import (47–50) (Table S1 and Figure 1A). CCNA_00028, CCNA_00027, and the CCNA_03155–03159 genetic locus are direct regulatory targets of the ferric uptake repressor Fur (30, 31), suggesting a connection between iron homeostasis and EDTA resistance at the tested concentration (300 μM).

Phenotypic effects of mutations in several zinc uptake regulator (Zur)-regulated genes have previously been reported in *C. crescentus* at higher EDTA concentrations (500 μM and 800 μM) on solid M2 defined medium (32). However, disrupting genes in the Zur regulon (32) individually did not have noteworthy fitness defects in our EDTA Tn-seq experiment except for *zrpW* (CCNA_00322), which encodes an uncharacterized transmembrane protein: *zrpW* mutants showed a small (factor ~1.5) reduction in fitness in the presence of 300 μM EDTA (Table S1; see Materials and Methods for fitness calculation method). Disruption of genes reported to support fitness under copper-induced stress (51–53) also did not strongly affect fitness except for *cobT* (CCNA_01367), encoding a predicted component of the cobaltochelatase complex involved in vitamin B_{12} biosynthesis. Strains harboring transposon insertions in the uranium/zinc/copper-responsive regulatory system (*uzcRS;* homologous to *E. coli cusRS*) (33) had a basal fitness defect in liquid medium alone that was rescued by treatment with EDTA. The *acrAB2/nodT* antibiotic resistance locus (54) is directly activated by the UzcRS two-component system (33), and insertional mutants in *acrAB2/nodT* had the largest EDTA rescue phenotype of all *C. crescentus* mutants, as indicated by their low fitness score in the absence of EDTA and their normal score in the presence of EDTA (Figure 1A and Table S1). In contrast, strains with insertions in *tipR*, the transcriptional repressor of *acrAB2/nodT* (55, 56), displayed the opposite fitness profile, consistent with the known regulatory connection between these genes. The basal fitness defects of strains with insertions in sphingolipid biosynthesis genes (CCNA_01212, CCNA_01220, CCNA_01221, CCNA_01223) (57) were also rescued by the addition of EDTA to the growth medium. We conclude that genes with cell envelope and iron acquisition functions are key *Caulobacter* fitness determinants in the presence of 300 μM EDTA. Our observation that EDTA treatment rescues the mutant phenotypes of select cell envelope mutants suggests a complex interaction between metal ion homeostasis and cell envelope development mechanisms in *C. crescentus*.

CCNA_00027 (*cciO*) and CCNA_00028 (*cciT*) are co-conserved EDTA resistance genes

Given the strong and specific fitness defects seen for mutants of the two genes encoding a TBDT (CCNA_00028) and dioxygenase (CCNA_00027) in complex medium containing EDTA, we chose these genes for further study. There was no obvious functional relationship between these two gene families: TBDTs transport a diverse array of molecules across the outer membrane, while 2OG/Fe^{II}-dependent dioxygenases introduce diatomic oxygen into a range of substrates (58). However, both genes are directly regulated by Fur (30, 31) and are operonic (59), suggesting related function(s).

RB-TnSeq data (Table S1) could not differentiate whether the fitness defect ascribed to disruption of the TBDT gene (CCNA_00028) was due to a polar effect on the adjacent dioxygenase gene (CCNA_00027) or to the disruption of CCNA_00028 *per se* (see Figure 1B). To distinguish between these two possibilities and to validate the RB-TnSeq results, we constructed mutants carrying in-frame, unmarked deletions of *CCNA_00027* or *CCNA_00028*. We hereafter refer to these genes as *cciO* and *cciT*, respectively, for reasons we will explain below. Both in-frame deletion mutants grew like the WT strain in complex medium and failed to grow in the same medium with 300 μM EDTA added (Figure 1C), confirming the RB-TnSeq fitness measurements (Figure 1A; Table S1). The growth defect of each mutant in complex liquid medium containing EDTA was genetically complemented by ectopic expression of the deleted gene from its native promoter (Figure 1C), thus defining CciO and CciT as EDTA resistance factors.

We assessed the prevalence and conservation of *cciO* and *cciT* through a pangenome analysis that binned genes into orthologous clusters (60). A comparison of 69 *Caulobacter* isolates from diverse environments including water, soil, and plant-associated ecosystems identified a highly related cluster of dioxygenase genes that includes *cciO*, which was detected in all but one of the analyzed genomes. The TBDT gene cluster that included *cciT* was present in 80% of the analyzed genomes (Table S2). A gene neighborhood analysis (61) showed that *cciO* homologs are commonly located

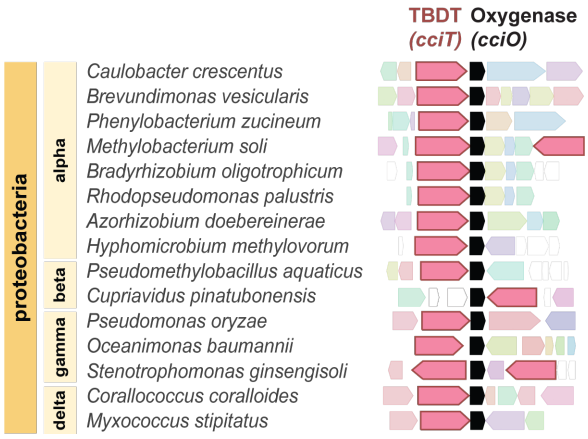

Figure 2. Orthologs of *cciT* and *cciO* are syntenic in Proteobacteria. Gene neighborhood analysis anchored on *cciO* reveals synteny of *cciO* and *cciT* orthologs. Neighborhood configuration was defined by selecting the highest-scoring BLAST hits from different proteobacterial groups and identifying the corresponding neighborhoods using webFLAGs (61). Representative genomes across the phylum Proteobacteria are presented. The *cciT* and *cciO* orthologs are colored in pink and black, respectively.

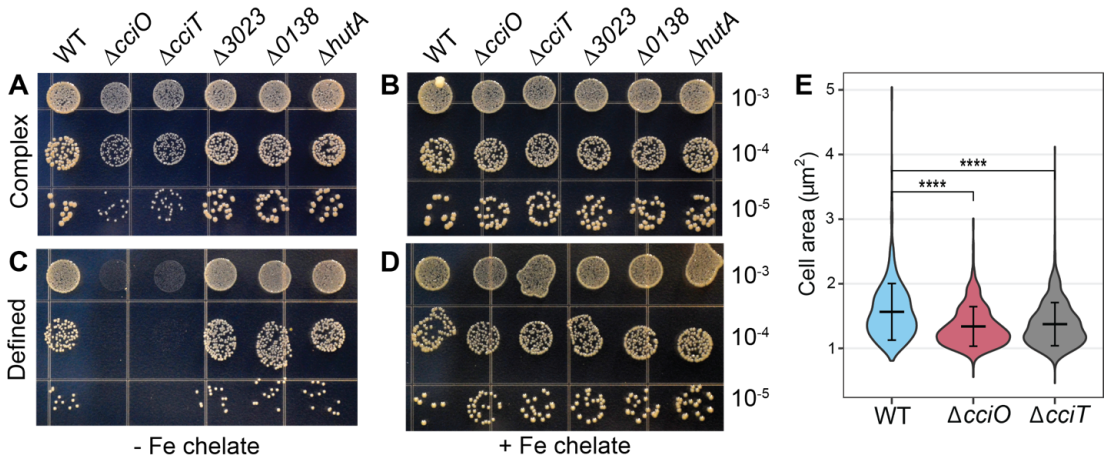

Figure 3. *cciT* and *cciO* deletion mutants have colony size and cell size phenotypes. Representative photographs of growth on plates for the WT strain, the Δ*cciO* deletion mutant, and deletion mutants for each of the Fur-regulated TonB-dependent transporter genes (Δ*cciT*, Δ*CCNA_00138*, Δ*CCNA_03023*, and Δ*hutA*) serially diluted and spotted onto complex (PYE; A & B) or defined (M2X; C & D) agar medium. The medium in B and D was supplemented with 10 μM Fe•EDTA chelate, whereas the medium in A and C was not. The dilution factor of each row is indicated at right. Panel E shows the distribution of cell areas in WT (n=759), Δ*cciO* (n=750), and Δ*cciT* (n=1154) cells grown in PYE broth for 6 hours. Comparisons between strains were made using Kruskal-Wallis test, followed by Dunn's test. **** $p < 0.0001$.

directly adjacent to *cciT* homologs in *Caulobacter* species and more broadly in the Proteobacteria (Figure 2). This high degree of synteny supports an evolutionary and functional relationship between *cciT* and *cciO*.

Growth defects of *cciO* and *cciT* mutants are rescued by chelated iron

Having identified *cciT* and *cciO* as EDTA resistance genes, we sought to define the functions of the proteins encoded by this co-conserved gene pair. The growth of Δ*cciO* and Δ*cciT* mutants in complex (PYE) liquid growth medium was equivalent to that of the WT strain (Figure S2A & Figure 1C). When we spotted ten-fold dilution series on solid PYE agar plates, we observed comparable numbers of colony-forming units (CFUs) for all strains, although Δ*cciO* and Δ*cciT* strains produced visibly smaller colonies (Figure 3A). The colony size defect was genetically complemented by expressing each of the deleted genes from an ectopic locus from its own promoter (Figure S3A). The fact that transcription of *cciO* and *cciT* is regulated by Fur (30, 31) indicated that the diminished growth on solid medium seen in their respective mutants might be a result of a defect in iron homeostasis. To test this hypothesis, we added 10 μM Fe•EDTA chelate to solid PYE agar medium, which restored the colony size of the mutants to WT levels (Figure 3B).

We tested strain growth in liquid M2X defined medium containing 10 μM Fe•EDTA as an iron source. The growth of the Δ*cciO* and Δ*cciT* mutants matched that of the WT strain in this condition (Figure S2B). Replacing chelated iron (as Fe•EDTA) with 10 μM $FeCl_3$ did not affect WT growth but resulted in attenuated growth of the Δ*cciO* and Δ*cciT* mutants (Figure S2B). The growth-attenuated Δ*cciO* and Δ*cciT* mutant cells were also ~25% smaller than WT ($p<0.0001$) in this liquid medium condition (Figure 3E). We conclude that *cciO* and *cciT* mutants have a decreased ability to acquire unchelated Fe^{III} in defined liquid medium. On defined solid (agar) medium without added iron, the WT *C. crescentus* strain had sufficient iron scavenging ability to grow well (Figure 3C), whereas growth of the Δ*cciO* and Δ*cciT* mutants was severely compromised. Again, this defect was rescued by the addition of 10 μM Fe•EDTA chelate (Figure 3D), indicating that both *cciO* and *cciT* support acquisition of iron from a defined solid medium. Accordingly, we named the constituent genes of this syntenic gene pair *C. crescentus* iron transporter (*CCNA_00028*; *cciT*) and *C. crescentus* iron oxygenase (*CCNA_00027*; *cciO*); we provide additional experimental data supporting a functional role for *cciT* and *cciO* in cellular iron homeostasis below.

Deletion of *cciT* or *cciO* de-represses transcription of the Fur regulon

To test the hypothesis that intracellular iron homeostasis is perturbed in Δ*cciT* and Δ*cciO*, we first measured global transcript levels by transcriptome deep sequencing (RNA-seq), reasoning that lower intracellular iron levels would manifest as de-repressed transcription of Fur-regulated genes. Deletion of *cciT* or *cciO* resulted in increased expression of a small and highly congruent gene set (Figure 4 and Table S3). Of the 24 genes differentially expressed in at least one of the mutants (absolute $\log_2$[fold change] > 1; FDR p-value < 10^{-4}), 17 had increased transcript levels in both mutants, and 21 had been demonstrated to be regulated in an iron-dependent manner in earlier studies (30, 62). Most genes with enhanced expression in Δ*cciT* and Δ*cciO* are known to be repressed by Fur (30, 31, 62), including *cciT* itself, three additional TBDT genes, and the predicted inner membrane ferrous iron transport system *feoAB*. To validate the RNA-seq results, we measured transcription using reporter constructs consisting of the fluorescent reporter gene *mNeonGreen* cloned downstream of the *cciT* or *feoAB* promoter. Consistent with the RNA-seq data, transcription from the *cciT* and *feoAB* promoter constructs was significantly de-repressed in Δ*cciT* and Δ*cciO* relative to WT (Figure S4A & B; Figure 4C).

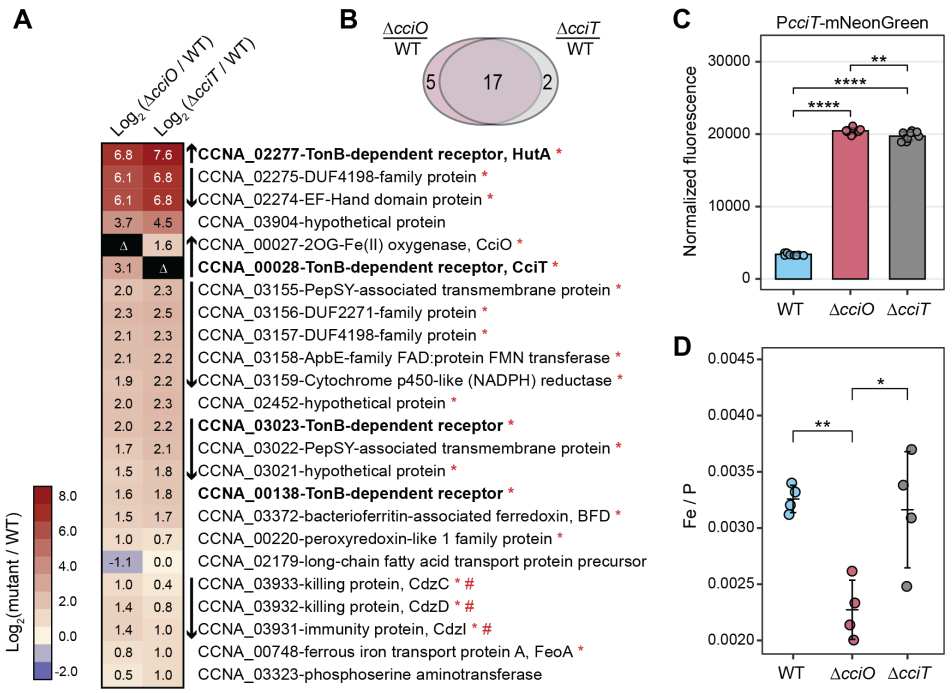

Figure 4. Δ*cciT* and Δ*cciO* mutants have an iron homeostasis defect. (A) Heatmap of expression of the 24 genes differentially transcribed in Δ*cciT* or Δ*cciO* strains, relative to WT cells, grown in defined medium containing $FeCl_3$ as a sole iron source. Each row represents one gene, each column represents a mutant compared to the WT culture, and the color of each cell reflects the magnitude of transcriptional change, as the log_2(mutant/WT) expression level (see key at left). Boldface indicates the TBDT genes directly repressed by Fur and upregulated during iron limitation. Vertical arrows between the heatmap and gene listings indicate the orientations of adjacent genes (presumed operon structures). Red asterisks indicate genes with a Fur-binding motif in their promoters (31). Differentially expressed genes in the mutants compared to the WT strain were defined as those with an absolute log_2(fold change) > 1 and a false discovery rate (FDR) p-value < 0.0001. (B) Venn diagram showing the extent of overlap between differentially expressed genes in each mutant compared to the WT strain. (C) Transcription from the *cciT* promoter (P_{cciT}) using a P*cciT*:mNeonGreen reporter plasmid in WT, Δ*cciT*, and Δ*cciO* strains grown in PYE complex medium (n = 9). Comparisons of normalized fluorescence were made with a Welch's ANOVA test followed by Tukey's multiple comparison test. Statistical significance was indicated as follows: **, $p < 0.01$; ****, $p < 0.0001$.(D) Inductively coupled plasma mass spectrometry (ICP-MS) quantification of total cellular ^{56}Fe, normalized to cellular phosphorus, in WT, Δ*cciT*, and Δ*cciO* strains grown in PYE complex medium. Comparisons of ^{56}Fe levels between mutant strains and the WT were performed using ANOVA, followed by Tukey's multiple comparison test. Statistical significance is indicated as follows: *, $p < 0.05$; **, $<p < 0.01$.

Additionally, we tested whether increased levels of *cciT* transcripts in *ΔcciO* led to increased CciT protein abundance in the outer membrane. Indeed, we detected significantly higher CciT protein levels in purified outer membranes of *ΔcciO* relative to the WT strain (Figure S4C &D) during iron limitation imposed by treatment with the intracellular iron chelator dipyridyl. This result supports the RNA-seq data and demonstrates that *ΔcciO* phenotypes are not due to diminished CciT production or to a defect in CciT localization.

cciT and *cciO* mutants are resistant to iron-dependent antimicrobial compounds

To further assess the consequences of *cciT* or *cciO* deletion on cellular iron homeostasis, we used a streptonigrin sensitivity assay. Streptonigrin toxicity increases with increasing intracellular iron levels (63, 64), and both *ΔcciO* and *ΔcciT* strains were less sensitive than WT cells to streptonigrin when grown on PYE agar (Figure 5A & 5C), supporting the hypothesis that intracellular iron concentrations are lower in these strains. Supplementing the medium with 10 μM Fe•EDTA returned mutant sensitivity to streptonigrin to WT levels (Figure 5A & 5C). As a complementary approach, we measured the sensitivity of WT, Δ*cciO*, and Δ*cciT* strains to the drug CHIR-090, which inhibits the lipid A biosynthesis enzyme, LpxC (65). Lipid A is typically an essential component of the Gram-negative outer membrane, but the de-repression of Fur-regulated transcription (which occurs during iron limitation) renders lipid A dispensable in *C. crescentus* (57). CHIR-090 toxicity is therefore predicted to be diminished when cells are iron-limited. Consistent with this hypothesis, the *ΔcciO* and *ΔcciT* mutants were both more resistant to CHIR-090 treatment than the WT. Again, addition of 10 μM Fe•EDTA to the medium sensitized the mutants to this antimicrobial compound (Figure 5B & 5C). These data provide independent, pharmacological lines of evidence that cells lacking CciO or CciT have lower intracellular iron levels than WT.

Direct measurement of cellular iron levels in *cciT* & *cciO* mutants

The transcriptomic and pharmacological experiments described above provide three independent lines of evidence that intracellular iron levels are lower in Δ*cciT* and Δ*cciO* cells (Figure 5). To directly measure the effect of *cciT* or *cciO* deletion on cellular iron levels, we turned to inductively coupled plasma triple-quadrupole mass spectrometry (ICP-MS-QQQ). While Δ*cciT* and Δ*cciO* cells exhibited highly

diminished growth and de-repressed transcription of Fur-regulated genes in a defined medium supplemented with $FeCl_3$, ferric oxides in the cell pellets confounded our cellular iron measurements in this condition. We therefore tested whether iron levels were basally affected in the Δ*cciT* and Δ*cciO* mutants cultivated in a complex medium. Iron abundance data were first normalized to colony forming units (atoms/CFU) (Figure S5). To more accurately assess differences between strains, we further normalized the element concentration data to the levels of phosphorus in each sample, which is an established internal standard (66). Phosphorus-normalized iron levels were significantly lower in Δ*cciO* ($p < 0.007$), with approximately 30% less iron than WT cells (Figure 4C). Δ*cciT* normalized iron levels were more variable than either WT or Δ*cciO*, but did not significantly differ from the WT strain. This result, when considered alongside the transcriptomic data (Figure 4A) and pharmacological data (Figure 5), supports a model in which Δ*cciT* cells can bind iron but not efficiently import it. We discuss this model below.

CciT and CciO coordinately function as a major iron-acquisition system in complex and defined media

Deletion of *cciT* or *cciO* decreased intracellular iron levels, but *cciT* is only one of four Fur-regulated TBDT genes that are transcriptionally activated in response to iron limitation in complex medium (30). We therefore tested whether and how the remaining Fur-regulated TBDT genes might contribute to *C. crescentus* fitness under our assay conditions. To this end, we generated mutant strains lacking each of the other three Fur-regulated TBDT genes: CCNA_00138, CCNA_03023, and CCNA_02277 (previously named *hutA* (67). Growth of these single TBDT mutants was equivalent to that of WT cells on solid complex or solid defined medium, regardless of iron supplementation (Figure 3). Thus, the Δ*cciT* mutant was the only mutant in a Fur-regulated TBDT gene to exhibit a growth defect on solid medium.

To more rigorously define the contributions of the four Fur-regulated TBDTs to *C. crescentus* growth and to test the hypothesis that CciT acts as the main outer membrane iron importer in both complex PYE and defined M2X media, we developed a new set of mutan t strains with deletions in three of the four Fur-regulated TBDT genes, leaving only one Fur-regulated TBDT gene intact in each strain (ΔΔΔ*cciT*$^+$, ΔΔΔ*138*$^+$, ΔΔΔ*3023*$^+$, and ΔΔΔ*hutA*$^+$). We also generated a quadruple deletion strain lacking all four Fur-regulated TBDT genes (ΔΔΔΔ). All strains had similar growth kinetics in liquid PYE medium during the exponential phase, indicating that *C. crescentus* can acquire iron through other transport systems in complex medium (Figure S2C). On solid complex medium, all triple deletion strains retaining only one active single transporter yielded comparable CFU numbers across serial dilutions, although only the ΔΔΔ*cciT*$^+$ triple mutant had a colony size similar to that of WT cells (Figure 6A). The growth benefit provided by *cciT* was particularly evident on solid M2 defined medium without added iron, where the growth of strains ΔΔΔ*138*$^+$, ΔΔΔ*3023*$^+$, and ΔΔΔ*hutA*$^+$ was diminished while that of ΔΔΔ*cciT*$^+$ matched

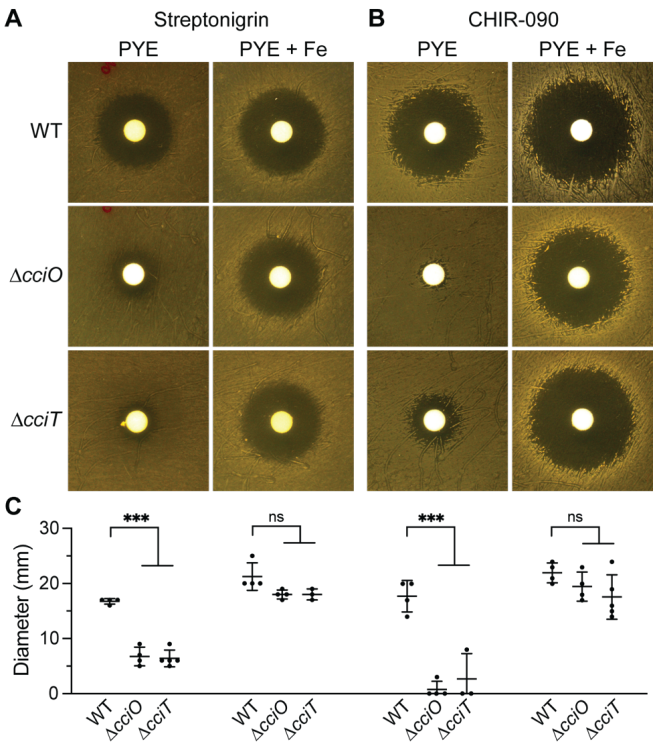

Figure 5. Δ*cciO* and Δ*cciT* mutants are resistant to streptonigrin and CHIR-090. WT, Δ*cciO*, Δ*cciT* were spread onto solid PYE medium without or with 10 μM Fe•EDTA and challenged with diffusion disks loaded with (A) streptonigrin or (B) CHIR-090. (C) Diameters of the zones of inhibition after growth for the plates shown in (A) and (B). The mean ± standard deviation of at least three independent experiments are overlayed with the individual data points. For each growth condition, the inhibitory zones were compared using analysis of variance (ANOVA) followed by a Dunnett's post-hoc test. not significant, ns, $p > 0.01$; *** $p < 0.001$.

the growth of the WT strain (Figure 6C). Growth of the quadruple TBDT gene deletion strain (ΔΔΔΔ) was severely compromised relative to the WT strain on solid complex and defined media (Figure 6A & C). We conclude that at least one of the four Fur-regulated TBDT genes is required for growth on solid medium, and that CciT alone is sufficient to confer WT-like growth. Supplementation of the medium with 10 μM Fe•EDTA chelate completely rescued the growth of all strains except the ΔΔΔΔ strain, which was only partially rescued by this concentration of EDTA-chelated iron (Figure 6B & D). Thus, *C. crescentus* can acquire iron from Fe•EDTA through a system distinct from the four TBDTs studied here. Robust chemical rescue of the strains retaining a single Fur-regulated TBDT gene by 10 μM Fe•EDTA provides evidence that each of these TBDTs can support acquisition of iron from Fe•EDTA at a concentration of 10 μM (Figure 6B & D).

CciT transporter function requires the CciO dioxygenase

CciO is commonly encoded from a chromosomal locus adjacent to *cciT* in Proteobacteria (Figure 2) and has a functional role in the maintenance of cellular iron levels (Figures 4–6). Given the similar growth phenotypes of strains lacking either *cciT* or *cciO* (Figures 3, 5, 6 & S2), we postulated that the CciO dioxygenase was specifically required for CciT-supported growth. To assess the functional relationship between *cciO* and *cciT*, we deleted *cciO* from the triple TBDT deletion strain, retaining *cciT* as the only intact

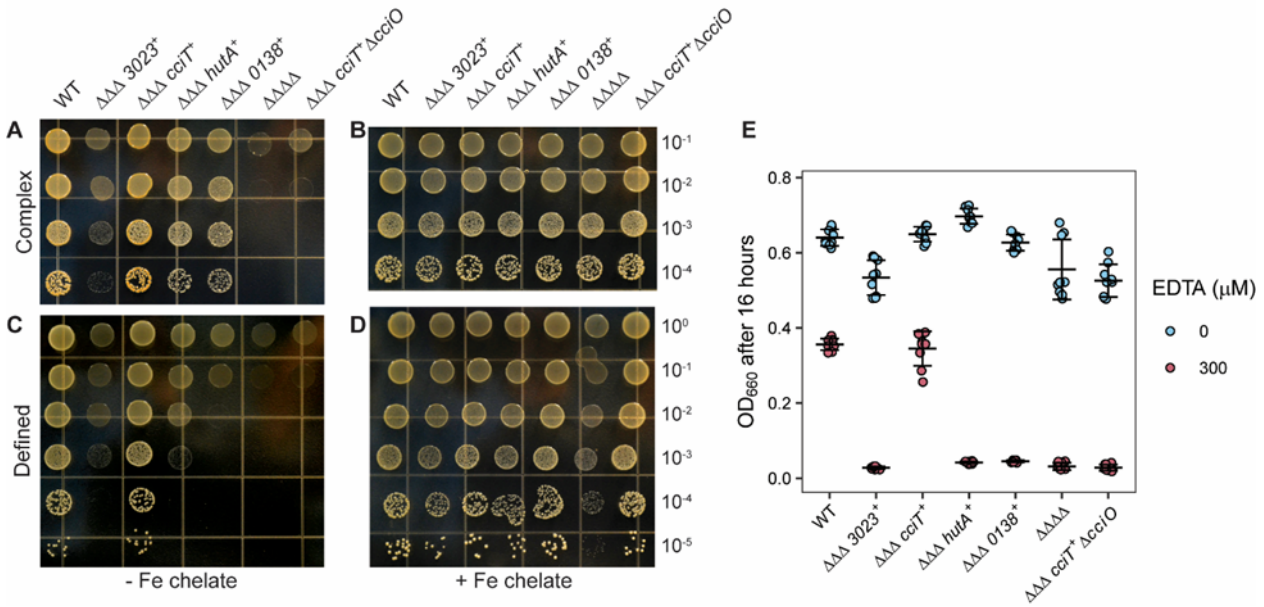

Figure 6. *cciT* alone is sufficient to support wild type-like growth on solid medium; this function requires *cciO*. WT, strains lacking three of the four Fur-regulated TBDT genes (ΔΔΔ CCNA_03023+, ΔΔΔ *cciT*+, ΔΔΔ *hutA*+, and ΔΔΔ CCNA_00138+), and a strain lacking all four Fur-regulated TBDT genes (ΔΔΔΔ) were serially diluted 10-fold and spotted onto solidified complex PYE medium (**A**, **B**) or defined M2X medium (**C**, **D**), without (**A**, **C**) or with 10 μM Fe•EDTA (**B**, **D**). (**E**) Optical density at 600 nm of all strains after growth for 16 h in complex liquid PYE medium without (blue) or with 300 μM EDTA (pink). The mean ± standard deviation of three independent trials of three independent cultures (n = 9), are overlayed with the individual data points.

TBDT gene (designated ΔΔΔ *cciT*+ Δ*cciO*). The growth defect of this strain was comparable to that of the ΔΔΔΔ strain lacking all four Fur-regulated TBDT genes when grown on complex solid medium, defined solid medium, and in liquid defined medium (Figures 6 and S2D). Thus, the ability of CciT to support *Caulobacter* growth requires CciO. To determine if the function of CciO is specific to the CciT transporter or if it plays a broader role in iron acquisition, we deleted *cciO* in other mutant strains harboring only one of the four Fur-regulated TBDT genes. We thus generated the strains ΔΔΔ *138*+ Δ*cciO*, ΔΔΔ *3023*+ Δ*cciO*, and ΔΔΔ *hutA*+ Δ*cciO*. The growth advantage provided by each of these single transporter genes was unaffected by deletion of *cciO* (Figure S3). We conclude that there is a specific iron transport relationship between the dioxygenase CciO and the TonB-dependent transporter CciT.

CciT and CciO support iron acquisition under chelation stress

CciT and CciO are EDTA resistance factors that function together as a major *C. crescentus* iron-acquisition system. However, the mechanism by which EDTA treatment compromised growth of the *cciT* and *cciO* mutants remained unclear. To address this question, we first queried the specific contribution of each Fur-regulated TBDT gene to EDTA resistance by measuring growth in complex (PYE) liquid medium containing 300 μM EDTA. CciT fully and uniquely supported *C. crescentus* growth at this EDTA concentration, and its ability to execute this function required *cciO* (Figure 6E). To assess the relative iron-acquisition ability of WT, Δ*cciO*, and Δ*cciT* strains in complex liquid medium containing 300 μM EDTA, we added increasing concentrations of $FeCl_3$ (1, 10, 50, and 100 μM) to the liquid medium and measured growth. Supplementation with $FeCl_3$ enhanced the growth of all strains in a dose-dependent manner (Figure 7A), but to different degrees, pointing to differences in Fe requirements as a function of genotype. Indeed, the addition of as little as 10 μM FeCl3 was sufficient to maximize the growth enhancement of WT cultures, whereas the growth of the Δ*cciO* and Δ*cciT* cultures was only modestly enhanced at this concentration. The Δ*cciO* and Δ*cciT* mutant strains required five times more ferric iron (50 μM $FeCl_3$) than WT to achieve near maximal growth enhancement. We conclude that the addition of 300 μM EDTA to the medium impairs the ability of *cciT* and *cciO* mutants to acquire ferric iron.

EDTA treatment was reported to lower the level of cellular iron, manganese, and zinc in *E. coli* (16). Transcriptional reporter assays showed that EDTA treatment increases transcription of Fur-regulated genes in the WT *C. crescentus* strain (Figure 7B & C), and that EDTA-induced iron limitation is more severe in Δ*cciO* and Δ*cciT* mutants, as we detected higher normalized fluorescence from the reporters in the mutant backgrounds than in WT (Figures 1C, 7B & C). While *C. crescentus* can use Fe•EDTA as an iron source, we propose that CciT–CciO enables transport of an undefined Fe^{III}-siderophore complex at a lower concentration than iron from Fe•EDTA. From this model, we predicted that adding a chelated iron source that is transported through an alternative high-affinity transport system would rescue the growth defects of strains lacking the CciO–CciT system when EDTA is present. Indeed, adding 1 μM of hemin—an iron-porphyrin complex transported by HutA (67)—partially restored the growth of the Δ*cciO* and Δ*cciT* mutant strains cultivated in a complex medium with 300 μM EDTA (Figure 7A), while 10 μM hemin restored growth to WT levels. We further tested this model using the hydroxamate

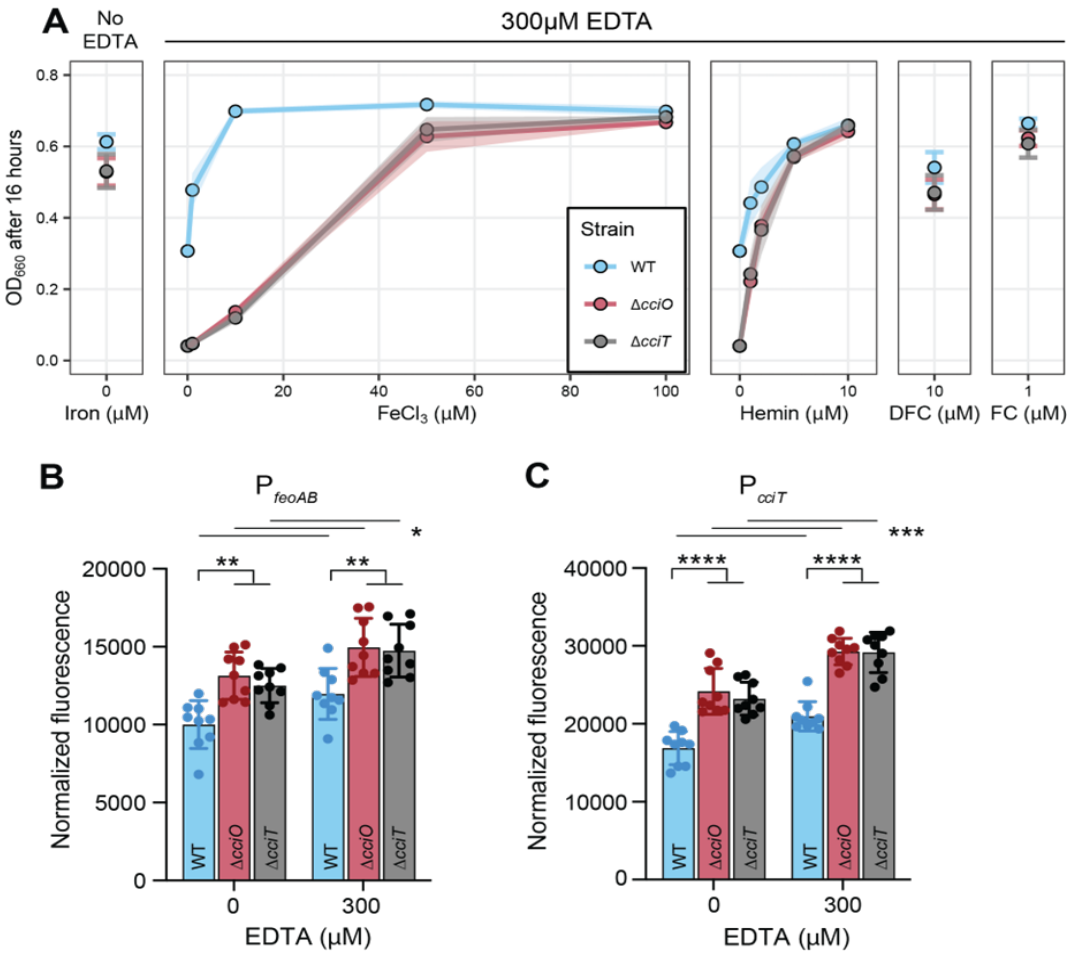

Figure 7. *ΔcciO* and *ΔcciT* have diminished ferric iron–acquisition ability in the presence of EDTA. (A) Optical density at 600 nm of WT, *ΔcciO*, and *ΔcciT* strains after 16 h of growth in PYE medium without (far left) or with 300 μM EDTA (center and right) with increasing concentrations of $FeCl_3$ or hemin, 10 μM desferrichrome (DFC), or 1 μM ferrichrome (FC) as indicated on the X-axis. Values represent mean ± SD (as shaded area) of at least six independent replicates. **(B&C)** Fluorescence output (normalized to cell density) of WT, *ΔcciO*, and *ΔcciT* strains carrying an *mNeonGreen* reporter cassette under the control of the Fur-regulated *feoAB* **(B)** or *cciT* promoters **(C)**. Cells were grown for 1.5 hours in liquid PYE medium without or with 300 μM EDTA. Values are means ± SD of 9 independent cultures assayed over three different days.Iindividual data points are also shown. A two-way ANOVA followed by Tukey's post-hoc test was used to assess differences between strains (lower brackets) and between treatments (upper lines). * $p < 0.05$; ** $p < 0.01$, *** $p < 0.001$, **** $p < 0.0001$).

siderophore desferrichrome (DFC), which is efficiently transported by *C. crescentus* at sub-nanomolar concentrations (67). DFC has a higher overall stability constant with Fe^{III} than EDTA (68) and can thus compete with EDTA for available ferric iron in the medium. Adding 10 μM desferrichrome to a complex liquid medium containing 300 μM EDTA restored the growth of the mutant strains to near WT levels, while adding 1 μM of DFC pre-loaded with Fe^{III} (i.e. ferrichrome, FC) fully rescued the growth of the Δ*cciO* and Δ*cciT* mutants challenged with 300 μM EDTA (Figure 7A).

Assessing the role of the CciT–CciO system in the import of catechol siderophores

A phylogenetic analysis of *C. crescentus* and *E. coli* TBDTs revealed a close relationship between CciT and Fiu (67), which transports monomeric catechol-based siderophores in *E. coli* (69). As presented above, Fiu is encoded from a locus adjacent to a 2OG/Fe^{II}-dependent dioxygenase gene homologous to *cciO* and functions as the outer membrane transporter for the catechol-cephalosporin antibiotic cefiderocol (67). A function for *C. crescentus* CciT as a Fiu/PiuA-like catechol transporter would imply that deletion of *cciT* would result in cefiderocol resistance, as reported in resistant clinical isolates of several bacterial pathogens (35, 70). Unexpectedly, wild-type *C. crescentus* was highly resistant to cefiderocol treatment, and deletion of either *cciT* or *cciO* increased this sensitivity (Figure S6). Supplementing the medium with 10 μM Fe•EDTA attenuated the cefiderocol sensitivity of the mutants. We conclude that CciT does not transport cefiderocol and propose that another transport system, upregulated upon iron limitation in the Δ*cciO* and Δ*cciT* mutant backgrounds, transports this catechol-containing antibiotic into *Caulobacter* cells. This unknown cefiderocol/catechol transport system is apparently not one of the other three Fur-regulated TBDTs, as the strains harboring a single Fur-regulated TBDT gene and the quadruple deletion strain (ΔΔΔΔ) were all sensitive to cefiderocol (Figure S7).

We tested other known catecholate siderophores as possible CciT substrate(s), including 2,3′-dihydroxybenzoic acid (2,3-DHBA) (69), chlorogenic acid (66), and protocatechuate (3,4-DHBA), which is known to be catabolized by *C. crescentus* (72). In a defined liquid medium, addition of

Fe^{III} complexed with any of these three catecholates at a 1 μM Fe^{III}:10 μM catecholate ratio enhanced growth of all single TBDT gene deletion strains relative to 1 μM Fe^{III} provided as $FeCl_3$, although iron complexed to 2,3-DHBA or chlorogenic acid enhanced growth more than protocatechuate (Figure S8). The growth phenotype of ΔΔΔ*cciT*$^+$Δ*cciO* matched that of the ΔΔΔΔ strain in most conditions, consistent with a model in which CciT function requires CciO. The one exception was in medium containing Fe^{III} mixed with 2,3-DHBA, where catechol-enhanced growth did not require *cciO* (Figure S8).

The cefiderocol resistance and Fe^{III}-catecholate growth supplementation data provided evidence that *C. crescentus* can transport catecholates through multiple routes at the tested concentrations. A specific growth enhancement of a particular strain (or strains) carrying single Fur-regulated TBDT genes was not evident for any of the tested catecholates (Figure S8B), and the data clearly show that the *cciT–cciO* locus conferred the greatest growth advantage under conditions with no added iron. This result indicates that the CciT–CciO system either supports acquisition of some form of chelated iron present in M2 defined medium or that CciT transports a siderophore produced by *C. crescentus* itself, a possibility that we discuss below.

Growth and EDTA sensitivity of Δ*cciO* and Δ*cciT* in a natural environment context

The *cciT–cciO* locus encodes a major *C. crescentus* iron-acquisition system that supports fitness and EDTA resistance in traditional laboratory media, but the natural environment of *Caulobacter* spp. is aquatic and soil ecosystems (19). As such, we assessed the consequences of *cciT–cciO* gene deletion and EDTA treatment on *C. crescentus* growth in *bona fide* freshwater collected from two lakes in Michigan, USA: a developed recreational lake (Lake Lansing) and a Laurentian Great Lake (Lake Huron). A previous genome-scale analysis of *C. crescentus* mutant strains cultivated in water collected from Lake Michigan, which is part of the same lake system as Lake Huron, provided evidence that shore water can be approximated by highly diluted complex medium (39). We postulated that EDTA would therefore inhibit *C. crescentus* growth in lake water, as in standard complex liquid medium (PYE). To test this prediction, we cultivated the WT, *ΔcciO*, and *ΔcciT* strains in water collected from both Lake Lansing and Lake Huron alone or with 300 μM EDTA added and measured their growth by enumerating CFU. The populations of *C. crescentus* cells grown in these natural water samples underwent ~6–8 doublings, reaching a higher density in water collected from Lake Lansing compared to that from Lake Huron (Figure 8). Phosphorus levels were similar between lake samples (Figure S8 and Table S4), but total organic carbon (7.7 versus 4.5 mg/mL) and Kjeldahl nitrogen levels (0.80 versus 0.33 mg/mL) were higher in water samples from Lake Lansing (Table S5), which likely explains higher levels of *C. crescentus* growth in those water samples. Surprisingly, we observed no significant differences in growth between WT cells and the *ΔcciO* or *ΔcciT* mutant strains in these lake water samples regardless of 300 μM EDTA addition, suggesting that *C. crescentus* (a) is less sensitive to chelation stress in *bona fide* freshwater conditions and (b) can use other iron sources in these freshwaters beyond the form of iron that is imported by the CciT–CciO system.

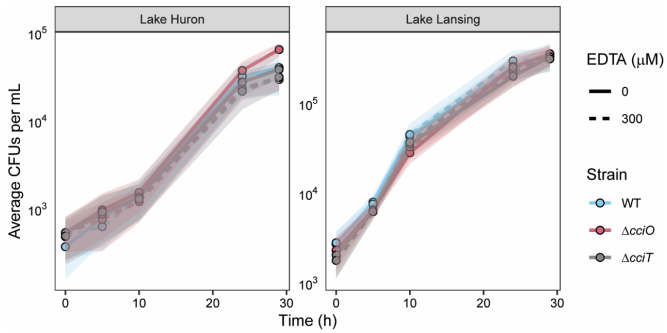

Figure 8. Growth of mutant strains in water collected from Lake Huron and Lake Lansing is not affected by the addition of EDTA. WT, *ΔcciO*, and *ΔcciT* strains inoculated into water collected from Lake Huron (left) or Lake Lansing (right) that was filtered before inoculation, with (dashed lines) and without (solid lines) 300 μM EDTA added. CFUs were enumerated after 0, 5, 10, 24, and 29 h of growth. Values represent means ± SD (as shaded areas) of three replicate cultures generated on the same day.

Quantitative elemental analysis of growth media and the relationship between cation profile and EDTA toxicity

We considered how differences in the chemistry of laboratory media and lake water samples may contribute to the differential growth and EDTA sensitivity of *C. crescentus* across these environments, and therefore determined the elemental profiles of non-supplemented liquid M2X defined medium, liquid PYE complex medium, and water collected from the two lakes by ICP-MS-QQQ. M2X contained the expected concentrations of the major medium components (Figure S8 and Table S4). Sodium, potassium, and phosphorus levels were ~2–10 times lower in PYE medium relative to M2X, although the levels in PYE were still ~3–30 times higher than in lake water (Table S4 and Figure S9). Sulfur levels were the highest in PYE medium (~2 mM) among all tested media and were substantially lower in the lake water samples. A difference in sulfur content between Lake Lansing and Lake Huron was reflected by the higher levels of measured sulfate ion in Lake Huron water samples (16 mg/L) relative to those from Lake Lansing (<5 mg/L). The contents of magnesium, copper, nickel, zinc, cobalt, chromium, selenium, and iron were all higher in PYE medium than in M2X medium and lake water. The level of iron in non-supplemented M2X defined medium approximated that measured in the water samples from Lake Lansing (80 nM) and Lake Huron (187 nM), while the concentration of iron in PYE medium was significantly higher (635 nM). Calcium concentrations in the lake waters were ~700 μM, which is congruent with that in PYE medium and ~2 times higher than in M2X medium. The toxic metals chromium and cadmium were more abundant in laboratory media than in the lake waters (Table S4 and Figure S9). Cadmium levels were substantially higher (by a factor of 16) in M2X defined medium than in complex PYE medium and were below the instrument detection limit in the lakes.

EDTA is a broad-spectrum metal chelator that can perturb the availability of many cations. Thus, the particular cation profile of a medium will influence the effect of EDTA on bacterial growth. We examined whether supplementing select cations could counteract the detrimental effects of 300 μM EDTA on *C. crescentus* growth in liquid PYE complex medium. Adding 2 mM Ca^{2+} or 1 μM Fe^{3+} partially rescued growth in the presence of EDTA. Similarly, the addition of 300 μM Zn^{2+}, Mn^{2+}, or Ni^{2+} also mitigated the growth-limiting effect of EDTA, although the addition of Zn^{2+} or Ni^{2+} alone (without EDTA) was toxic to *Caulobacter* (Figure S10). We propose that the combination of free cations and the efficient transport of chelated iron forms present in the lakes (e.g., ferrichrome or heme) contributes to the lower toxicity of EDTA in lake water samples. Future studies are needed to define the complex interplay between *Caulobacter*, iron, EDTA, and other cations in laboratory media and in freshwater ecosystems.

Discussion

A forward genetic screen for *C. crescentus* genes that affect fitness in the presence of the broad-spectrum synthetic chelator EDTA uncovered a TonB-dependent transporter (CciT) and a 2OG/Fe^{II}-dependent dioxygenase (CciO) that coordinately function to support cellular iron homeostasis. Our study defines *cciT–cciO* as encoding key iron-acquisition proteins and demonstrates the importance of these co-conserved, Fur-regulated genes in sustaining microbial growth under iron limitation and chelation stress.

Caulobacter has multiple routes through which it can acquire iron (67), but the CciT–CciO system provides the largest fitness advantage of all the Fur-regulated iron-acquisition systems in both complex and defined media. Deletion of any other Fur-regulated TBDT gene had no effect on growth (Figure 3), and no other single Fur-regulated TBDT besides CciT was sufficient to support WT-like growth on laboratory media (Figures 6 and S2D). In a complex medium containing EDTA, CciT uniquely supported fitness among the Fur-regulated TBDTs. The function of CciT in these treatment conditions strictly required the presence of the dioxygenase gene *cciO* (Figure 6E).

Transcriptional signatures of iron limitation in ΔcciT and ΔcciO

Deletion of either gene in the *cciT-cciO* operon led to increased transcription of a small set of genes, most of which are repressed by Fur, including *cciT* and *cciO* themselves (Figure 4 and Table S3). Several of the regulated genes were previously shown to be activated in response to treatment with the iron chelator 2,2′-dipyridyl (DP) (62, 67), though the transcriptional response to *cciT* or *cciO* deletion was less pronounced than the acute iron starvation response induced by DP. These transcriptomic data support the conclusion that loss of *cciT* or *cciO* function leads to reduced intracellular iron levels in both complex and defined media.

Notably, several uncharacterized genes that were modestly but significantly upregulated in Δ*cciT* and Δ*cciO* strains compared to wild-type have been linked to iron acquisition in other genera. For instance, genes from a predicted operon encoding a flavin-dependent reductase, a PepSY-family membrane protein (COG3295), and DUF2271 and DUF4198 domain proteins (locus *CCNA_03155-03159*) were significantly upregulated. Transposon insertions in these genes, which are proposed to facilitate periplasmic ferric iron reduction (47), decreased *C. crescentus* fitness in the presence of EDTA (Fig. 1 and Table S1). Experimental data from *Vibrio cholerae* further support a role for these COG/DUF proteins in iron acquisition, with COG3295 protein VciB promoting Fe^{II} transport by facilitating Fe^{III} reduction (48, 49). Additionally, transcriptome data from *Alteromonas macleodii* suggest that DUF2271 and DUF4198 proteins are also involved in iron acquisition (50).

Quantitative elemental analysis of the environment

In an effort to understand the variable sensitivity of *C. crescentus* to loss of *cciT* or *cciO* function in different media environments, we determined the elemental profiles of the artificial and natural media in which strains were cultivated (Table S4). To our knowledge, this study provides the first quantitative inorganic analysis of *Caulobacter* cultivation media. These data, when viewed in the context of accompanying analytical data from two Michigan lakes that supported the growth of *C. crescentus* (Figure 8), offer an opportunity to reconsider effects of the growth media that are used to evaluate the physiology and ecology of this important environmental bacterium. While the balance of available carbon, nitrogen, and phosphorus was orders of magnitude higher in defined (M2X) and complex (PYE) media than in lake waters (Figure S9 and Table S5), the ensemble of inorganic elements varied considerably. Sodium,

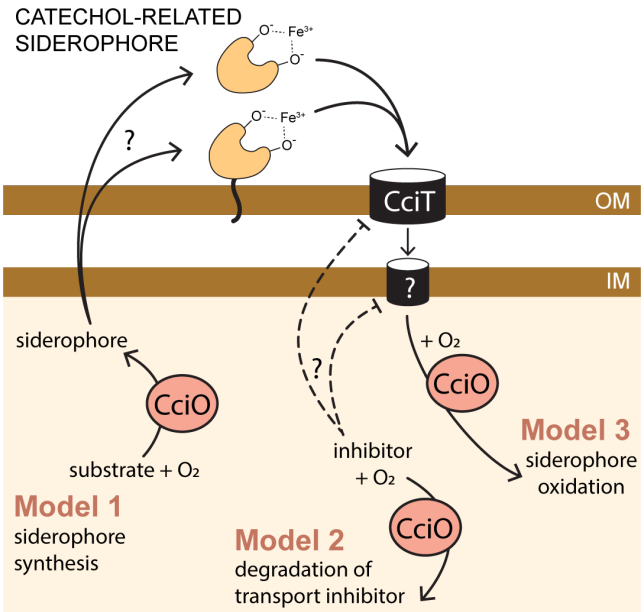

Figure 9: CciT and CciO function together to support iron homeostasis. *cciT* is a Fur-regulated gene encoding an outer membrane transporter related to known Fe^{III}•catechol transporters. Iron acquisition via CciT specifically requires CciO, a conserved dioxygenase. CciO may be required to synthesize the substrate of CciT (Model 1), degrade an inhibitor of CciT-dependent transport (Model 2), or oxidize the substrate of CciT (Model 3). The postulated iron-binding substrate of CciT may be cell-associated, as reported in many marine bacteria (89). The inner membrane transporter is not known.

potassium, sulfur, and nickel levels were 1–2 orders of magnitude higher in laboratory media than in waters of Lake Lansing or Lake Huron. The concentrations of essential metals including iron, magnesium, copper, cobalt, and zinc were comparable between lake water samples and M2X defined medium (without added iron supplements) but were 3–300 times higher in complex medium (Table S4 and Figure S8). Measured levels of calcium, manganese and molybdenum in the lakes were better reflected in complex medium than in defined medium. The levels of the toxic metals cadmium and chromium were both significantly higher in laboratory media than in the lake waters, which may influence *Caulobacter* physiology under certain experimental conditions. As the field continues to explore *Caulobacter* nutrient acquisition and stress physiology in environmental contexts, it may be useful to formulate media that have an inorganic composition that is more aligned with the composition of lake waters from this study.

Interactions of EDTA with Caulobacter and its growth medium

Experiments assessing the interactions between *C. crescentus*, EDTA, and its growth media have highlighted the redundancy and versatility of its iron-acquisition strategies. *C. crescentus* can use Fe•EDTA as an iron source (73), but we propose that *C. crescentus* does not utilize Fe•EDTA as efficiently, or at as low a concentration, as it does the *bona fide* substrate of CciT. In support of this model, we showed that CciT and CciO are strictly required for growth in a complex medium containing a concentration of EDTA that only partially limits growth of WT cells (Figure 6). We further demonstrated that *C. crescentus* CciT and CciO enable iron acquisition at low ferric iron concentrations, even when EDTA was present in high molar excess (Figure 7). Interactions between EDTA, the culture medium, and *Caulobacter* cells are complex and dependent on the chemical composition of the medium (Figure S10). Our data suggest redundancy in the ability of the multiple *Caulobacter* iron-acquisition systems to use not only Fe•EDTA but also a diverse set of Fe^{III}-catechol substrates when these compounds are available at low micromolar concentrations (Figures S6–S8). The CciT–CciO system is apparently the major iron import system in complex and defined laboratory media, but the WT-like growth phenotypes of the *ΔcciT* and *ΔcciO* mutants in lake water (with or without 300 μM EDTA) (Figure 8) reflect the adaptability of this common freshwater and soil microbe in acquiring essential nutrients in chemically complex natural habitats. The mechanism by which Lake Lansing and Lake Huron waters (effectively) buffer *Caulobacter* against EDTA treatment is not known, but there are almost certainly multiple chemical factors involved. The distinct metal ion profiles (Figures S9) and the highly complex array of inorganic and organic iron- and other metal-binding ligands present in natural waters (74–77), likely mitigate the biological effect of EDTA.

On the CciT/CciO substrate(s)

The outer membrane transporter CciT and the cytoplasmic dioxygenase CciO coordinately support robust growth of *C. crescentus* on both solid and liquid defined media (Figures 6 and S2). Given the strongly reduced growth of *ΔcciT* and *ΔcciO* relative to the WT strain in mineral defined media supplemented with $FeCl_3$, we propose that CciT imports ferric iron bound to a substrate that is not present in the medium and is produced by *C. crescentus* itself. The identity of this postulated compound is not known, but the evolutionary relationship between CciT, *E. coli* Fiu (67), and *Pseudomonas* spp. PiuA suggests that it would have a catecholate-like structure (Figure 9). Efforts to identify siderophore production by *C. crescentus* using colorimetric (78) and other analytical approaches have been unsuccessful to date, and the catechol supplementation and cefiderocol resistance data presented herein (Figures S6–S8) support the existence of multiple routes for catecholate entry at the tested concentrations.

The growth (Figures 3 & 6) and intracellular iron limitation phenotypes (Figure 5) of the *ΔcciO* strain matches those seen in *ΔcciT*, which provides evidence that the iron import function of CciT at the outer membrane requires the intracellular dioxygenase activity of CciO. Proteomic analysis of fractionated membranes demonstrated that CciT is produced and properly targeted to the outer membrane in the absence of CciO (Figure S3). Thus, a model in which CciT translation and/or targeting requires CciO activity can be ruled out. It is possible that CciO is involved in the biosynthesis of a siderophore, although we would not have expected to identify *cciO* mutants in our pooled RB-TnSeq screen (Figure 1) if CciO were required to synthesize a "shared good" that was secreted to the medium. If CciO is involved in the biosynthesis of an Fe^{III}-binding siderophore that is tethered to the outside of the cell as oberserved in some marine species (79) (Figure 9), then we may expect decreased fitness of *cciO* mutants in a pooled mutant screen, as we observed. A membrane-associated siderophore model is also consistent with ICP-QQQ-MS data showing reduced total cellular iron in Δ*cciO* but not in *ΔcciT* (Figure 4)

Homologs of CciO in *P. aeruginosa* and *E. coli* (known as PiuC or YbiX) have been suggested to transform the substrate transported by their respective adjacently encoded TBDT (80). CciO may participate in the catabolism of this postulated iron-bound siderophore, which could release the bound iron or help to sustain a favorable siderophore concentration gradient for import. Alternatively, CciT and CciO may not have the same (or even related) substrates. This study demonstrates a clear functional link between this widely co-conserved gene pair (Figure 2), and it is our hope that future studies will define the molecular connections between outer membrane iron transport and cytoplasmic dioxygenase activity.

References

1. Philippot L, Griffiths BS, Langenheder S. 2021. Microbial Community Resilience across Ecosystems and Multiple Disturbances. Microbiology and Molecular Biology Reviews 85:e00026-20.
2. Dodds WK, Zeglin LH, Ramos RJ, Platt TG, Pandey A, Michaels T, Masigol M, Klompen AML, Kelly MC, Jumpponen A, Hauser E, Hansen PM, Greer MJ, Fattahi N, Delavaux CS, Connell RK, Billings S,

Bever JD, Barua N, Agusto FB. 2020. Connections and Feedback: Aquatic, Plant, and Soil Microbiomes in Heterogeneous and Changing Environments. Bioscience 70:548–562.
3. Arango L, Buddrus-Schiemann K, Opelt K, Lueders T, Haesler F, Schmid M, Ernst D, Hartmann A. 2014. Effects of glyphosate on the bacterial community associated with roots of transgenic Roundup Ready soybean. Eur J Soil Biol 63:41–48.
4. Chen J, McIlroy SE, Archana A, Baker DM, Panagiotou G. 2019. A pollution gradient contributes to the taxonomic, functional, and resistome diversity of microbial communities in marine sediments. Microbiome 7:104.
5. Vitousek PM, Aber JD, Howarth RW, Likens GE, Matson PA, Schindler DW, Schlesinger WH, Tilman DG. 1997. Human alteration of the global nitrogen cycle: sources and consequences. Ecological Applications 7:737–750.
6. Seeley ME, Song B, Passie R, Hale RC. 2020. Microplastics affect sedimentary microbial communities and nitrogen cycling. Nat Commun 11:2372.
7. Parsaeimehr A, Miller CM, Ozbay G. 2023. Microplastics and their interactions with microbiota. Heliyon 9:e15104.
8. Huerta Lwanga E, Gertsen H, Gooren H, Peters P, Salánki T, van der Ploeg M, Besseling E, Koelmans AA, Geissen V. 2016. Microplastics in the Terrestrial Ecosystem: Implications for Lumbricus terrestris (Oligochaeta, Lumbricidae). Environ Sci Technol 50:2685–2691.
9. Bennett EM, Carpenter SR, Caraco NF. 2001. Human Impact on Erodable Phosphorus and Eutrophication: A Global Perspective: Increasing accumulation of phosphorus in soil threatens rivers, lakes, and coastal oceans with eutrophication. Bioscience 51:227–234.
10. McSweeney B, Day C. 2004. European Union Risk Assessment Report: EDETIC ACID (EDTA). Dortmund, Germany.
11. Finnegan S, Percival SL. 2015. EDTA: An Antimicrobial and Antibiofilm Agent for Use in Wound Care. Adv Wound Care (New Rochelle) 4:415–421.
12. Evstatiev R, Cervenka A, Austerlitz T, Deim G, Baumgartner M, Beer A, Krnjic A, Gmainer C, Lang M, Frick A, Schachner H, Khare V, Gasche C. 2021. The food additive EDTA aggravates colitis and colon carcinogenesis in mouse models. Sci Rep 11:5188.
13. Kołodyńska D. 2011. Chelating Agents of a New Generation as an Alternative to Conventional Chelators for Heavy Metal Ions Removal from Different Waste Waters, p. 339–370. *In* Ning, RY (ed.), Expanding Issues in Desalination. IntechOpen, Rijeka.
14. Schmidt CK, Fleig M, Sacher F, Brauch H-J. 2004. Occurrence of aminopolycarboxylates in the aquatic environment of Germany. Environmental Pollution 131:107–124.
15. Sillanpää M. 1997. Environmental Fate of EDTA and DTPA. Rev Environ Contam Toxicol 85–111.
16. Paterson JR, Beecroft MS, Mulla RS, Osman D, Reeder NL, Caserta JA, Young TR, Pettigrew CA, Davies GE, Williams JAG, Sharples GJ. 2022. Insights into the Antibacterial Mechanism of Action of Chelating Agents by Selective Deprivation of Iron, Manganese, and Zinc. Appl Environ Microbiol 88:e01641-21.
17. Leive L. 1965. Release of lipopolysaccharide by EDTA treatment of E. coli. Biochem Biophys Res Commun 21:290–6.
18. Colombari B, Alfano G, Gamberini C, Cappelli G, Blasi E. 2021. EDTA and Taurolidine Affect Pseudomonas aeruginosa Virulence In Vitro-Impairment of Secretory Profile and Biofilm Production onto Peritoneal Dialysis Catheters. Microbiol Spectr 9:e0104721.
19. Wilhelm RC. 2018. Following the terrestrial tracks of Caulobacter - redefining the ecology of a reputed aquatic oligotroph. ISME J 12:3025–3037.
20. Boutte CC, Srinivasan BS, Flannick JA, Novak AF, Martens AT, Batzoglou S, Viollier PH, Crosson S. 2008. Genetic and computational identification of a conserved bacterial metabolic module. PLoS Genet 4:e1000310.
21. Thanbichler M, Iniesta AA, Shapiro L. 2007. A comprehensive set of plasmids for vanillate- and xylose-inducible gene expression in Caulobacter crescentus. Nucleic Acids Res 35:e137–e137.
22. Stephens C, Christen B, Fuchs T, Sundaram V, Watanabe K, Jenal U. 2007. Genetic Analysis of a Novel Pathway for Xylose Metabolism in Caulobacter crescentus. J Bacteriol 189:2181–2185.
23. Wilhelm RC, Singh R, Eltis LD, Mohn WW. 2019. Bacterial contributions to delignification and lignocellulose degradation in forest soils with metagenomic and quantitative stable isotope probing. ISME J 13:413–429.
24. North H, McLaughlin M, Fiebig A, Crosson S. 2023. The Caulobacter NtrB-NtrC two-component system bridges nitrogen assimilation and cell development. J Bacteriol 205:e00181-23.
25. Berrios L, Ely B. 2021. Genes related to redox and cell curvature facilitate interactions between Caulobacter strains and Arabidopsis. PLoS One 16:e0249227.
26. Luo D, Langendries S, Mendez SG, De Ryck J, Liu D, Beirinckx S, Willems A, Russinova E, Debode J, Goormachtig S. 2019. Plant Growth Promotion Driven by a Novel Caulobacter Strain. Molecular Plant-Microbe Interactions 32:1162–1174.
27. Agler MT, Ruhe J, Kroll S, Morhenn C, Kim ST, Weigel D, Kemen EM. 2016. Microbial Hub Taxa Link Host and Abiotic Factors to Plant Microbiome Variation. PLoS Biol 14:e1002352.
28. Longley R. 2022. Impact Of Agricultural Management And Microbial Inoculation On Soybean (Glycine max) And Its Associated Microbiome. Michigan State University, East Lansing, Michigan.
29. Wetmore KM, Price MN, Waters RJ, Lamson JS, He J, Hoover CA, Blow MJ, Bristow J, Butland G, Arkin AP, Deutschbauer A. 2015. Rapid Quantification of Mutant Fitness in Diverse Bacteria by Sequencing Randomly Bar-Coded Transposons. mBio 6:e00306-15.
30. da Silva Neto JF, Lourenço RF, Marques M V. 2013. Global transcriptional response of Caulobacter crescentus to iron availability. BMC Genomics 14:549.
31. da Silva Neto JF, Braz VS, Italiani VCS, Marques M V. 2009. Fur controls iron homeostasis and oxidative stress defense in the oligotrophic alpha-proteobacterium Caulobacter crescentus. Nucleic Acids Res 37:4812–4825.
32. Mazzon RR, Braz VS, da Silva Neto JF, do Valle Marques M. 2014. Analysis of the Caulobacter crescentus Zur regulon reveals novel insights in zinc acquisition by TonB-dependent outer membrane proteins. BMC Genomics 15:734.
33. Park DM, Overton KW, Liou MJ, Jiao Y. 2017. Identification of a U/Zn/Cu responsive global regulatory two-component system in Caulobacter crescentus. Mol Microbiol 104:46–64.
34. Park DM, Overton KW, Jiao Y. 2019. The UzcRS two-component system in Caulobacter crescentus integrates regulatory input from diverse auxiliary regulators. Mol Microbiol 111:678–699.
35. Simner PJ, Beisken S, Bergman Y, Posch AE, Cosgrove SE, Tamma PD. 2021. Cefiderocol Activity Against Clinical Pseudomonas aeruginosa Isolates Exhibiting Ceftolozane-Tazobactam Resistance. Open Forum Infect Dis 8:ofab311.
36. Yamano Y, Ishibashi N, Kuroiwa M, Takemura M, Sheng W-H, Hsueh P-R. 2022. Characterisation of cefiderocol-non-susceptible Acinetobacter baumannii isolates from Taiwan. J Glob Antimicrob Resist 28:120–124.
37. Findlay J, Bianco G, Boattini M, Nordmann P. 2024. In vivo development of cefiderocol resistance in carbapenem-resistant Acinetobacter baumannii associated with the downregulation of a TonB-dependent siderophore receptor, PiuA. J Antimicrob Chemother 79:928–930.
38. Hall CM, Somprasong N, Hagen JP, Nottingham R, Sahl JW, Webb JR, Mayo M, Currie BJ, Podin Y, Wagner DM, Keim P, Schweizer HP. 2023. Exploring Cefiderocol Resistance Mechanisms in Burkholderia pseudomallei. Antimicrob Agents Chemother 67:e0017123.
39. Hentchel KL, Reyes Ruiz LM, Curtis PD, Fiebig A, Coleman ML, Crosson S. 2019. Genome-scale fitness profile of Caulobacter crescentus grown in natural freshwater. ISME Journal 13:523–536.
40. Hershey DM, Fiebig A, Crosson S. 2019. A Genome-Wide Analysis of Adhesion in Caulobacter crescentus Identifies New Regulatory and Biosynthetic Components for Holdfast Assembly. mBio 10:e02273-18.
41. Ohta N, Lane T, Ninfa EG, Sommer JM, Newton A. 1992. A histidine protein kinase homologue required for regulation of bacterial cell division and differentiation. Proceedings of the National Academy of Sciences 89:10297–10301.
42. Hershey DM, Fiebig A, Crosson S. 2021. Flagellar Perturbations Activate Adhesion through Two Distinct Pathways in *Caulobacter crescentus*. mBio 12:e03266-20.
43. Alakavuklar MA, Fiebig A, Crosson S. 2023. The Brucella Cell Envelope. Annu Rev Microbiol 77:233–253.
44. Anwari K, Poggio S, Perry A, Gatsos X, Ramarathinam SH, Williamson NA, Noinaj N, Buchanan S, Gabriel K, Purcell AW, Jacobs-Wagner

C, Lithgow T. 2010. A Modular BAM Complex in the Outer Membrane of the α-Proteobacterium Caulobacter crescentus. PLoS One 5:e8619.
45. Ryan KR, Taylor JA, Bowers LM. 2010. The BAM complex subunit BamE (SmpA) is required for membrane integrity, stalk growth and normal levels of outer membrane β-barrel proteins in Caulobacter crescentus. Microbiology (N Y) 156:742–756.
46. Noinaj N, Guillier M, Barnard TJ, Buchanan SK. 2010. TonB-dependent transporters: Regulation, structure, and function. Annu Rev Microbiol 64:43–60.
47. Méheust R, Huang S, Rivera-Lugo R, Banfield JF, Light SH. 2021. Post-translational flavinylation is associated with diverse extracytosolic redox functionalities throughout bacterial life. Elife 10:e66878.
48. Mey AR, Wyckoff EE, Hoover LA, Fisher CR, Payne SM. 2008. Vibrio cholerae VciB promotes iron uptake via ferrous iron transporters. J Bacteriol 190:5953–5962.
49. Peng ED, Payne SM. 2017. Vibrio cholerae VciB Mediates Iron Reduction. J Bacteriol 199:16.
50. Manck LE, Espinoza JL, Dupont CL, Barbeau KA. 2020. Transcriptomic Study of Substrate-Specific Transport Mechanisms for Iron and Carbon in the Marine Copiotroph Alteromonas macleodii. mSystems 5:e00070-20.
51. Maertens L, Cherry P, Tilquin F, Van Houdt R, Matroule JY. 2021. Environmental conditions modulate the transcriptomic response of both Caulobacter crescentus morphotypes to cu stress. Microorganisms 9.
52. Lawarée E, Gillet S, Louis G, Tilquin F, Le Blastier S, Cambier P, Matroule J-Y. 2016. Caulobacter crescentus intrinsic dimorphism provides a prompt bimodal response to copper stress. Nat Microbiol 1:16098.
53. Price MN, Wetmore KM, Waters RJ, Callaghan M, Ray J, Liu H, Kuehl J V, Melnyk RA, Lamson JS, Suh Y, Carlson HK, Esquivel Z, Sadeeshkumar H, Chakraborty R, Zane GM, Rubin BE, Wall JD, Visel A, Bristow J, Blow MJ, Arkin AP, Deutschbauer AM. 2018. Mutant phenotypes for thousands of bacterial genes of unknown function. Nature 557:503–509.
54. Kirkpatrick CL, Viollier PH. 2014. Synthetic interaction between the TipN polarity factor and an AcrAB-family efflux pump implicates cell polarity in bacterial drug resistance. Chem Biol 21:657–65.
55. Costafrolaz J, Panis G, Casu B, Ardissone S, Degeorges L, Pilhofer M, Viollier, PH. 2023. Adaptive β-lactam resistance from an inducible efflux pump that is post-translationally regulated by the DjlA co-chaperone. PLoS Biol 21: e3002040.
56. Kirkpatrick CL, Viollier PH. 2014. Synthetic Interaction between the TipN Polarity Factor and an AcrAB-Family Efflux Pump Implicates Cell Polarity in Bacterial Drug Resistance. Chem Biol 21:657–665.
57. Zik JJ, Yoon SH, Guan Z, Stankeviciute Skidmore G, Gudoor RR, Davies KM, Deutschbauer AM, Goodlett DR, Klein EA, Ryan KR. 2022. Caulobacter lipid A is conditionally dispensable in the absence of fur and in the presence of anionic sphingolipids. Cell Rep 39:110888.
58. Herr CQ, Hausinger RP. 2018. Amazing Diversity in Biochemical Roles of Fe(II)/2-Oxoglutarate Oxygenases. Trends Biochem Sci 43:517–532.
59. Bharmal M-H, Aretakis JR, Schrader JM. 2020. An Improved Caulobacter crescentus Operon Annotation Based on Transcriptome Data. Microbiol Resour Announc 9: e01025-20. 10.1128/mra.01025-20.
60. Eren AM, Kiefl E, Shaiber A, Veseli I, Miller SE, Schechter MS, Fink I, Pan JN, Yousef M, Fogarty EC, Trigodet F, Watson AR, Esen ÖC, Moore RM, Clayssen Q, Lee MD, Kivenson V, Graham ED, Merrill BD, Karkman A, Blankenberg D, Eppley JM, Sjödin A, Scott JJ, Vázquez-Campos X, McKay LJ, McDaniel EA, Stevens SLR, Anderson RE, Fuessel J, Fernandez-Guerra A, Maignien L, Delmont TO, Willis AD. 2021. Community-led, integrated, reproducible multi-omics with anvi'o. Nat Microbiol 6:3–6.
61. Saha CK, Sanches Pires R, Brolin H, Delannoy M, Atkinson GC. 2021. FlaGs and webFlaGs: discovering novel biology through the analysis of gene neighbourhood conservation. Bioinformatics 37:1312–1314.
62. Leaden L, Silva LG, Ribeiro RA, dos Santos NM, Lorenzetti APR, Alegria TGP, Schulz ML, Medeiros MHG, Koide T, Marques M V. 2018. Iron deficiency generates oxidative stress and activation of the sos response in Caulobacter crescentus. Front Microbiol 9: doi.org/10.3389/fmicb.2018.02014.
63. Hassett DJ, Britigan BE, Svendsen T, Rosen GM, Cohen MS. 1987. Bacteria form intracellular free radicals in response to paraquat and streptonigrin. Demonstration of the potency of hydroxyl radical. Journal of Biological Chemistry 262:13404–13408.
64. Yeowell HN, White JR. 1982. Iron requirement in the bactericidal mechanism of streptonigrin. Antimicrob Agents Chemother 22:961–8.
65. Barb AW, McClerren AL, Snehelatha K, Reynolds CM, Zhou P, Raetz CRH. 2007. Inhibition of Lipid A Biosynthesis as the Primary Mechanism of CHIR-090 Antibiotic Activity in Escherichia coli. Biochemistry 46:3793–3802.
66. Lane A, Gokhale A, Werner E, Roberts A, Freeman A, Roberts B, Faundez V. 2022. Sulfur- and phosphorus-standardized metal quantification of biological specimens using inductively coupled plasma mass spectrometry. STAR Protoc 3:101334.
67. Balhesteros H, Shipelskiy Y, Long NJ, Majumdar A, Katz BB, Santos NM, Leaden L, Newton SM, Marques M V., Klebba PE. 2017. TonB-dependent heme/hemoglobin utilization by Caulobacter crescentus HutA. J Bacteriol 199:e00723-16.
68. Anderegg G, L'Eplattenier F, Schwarzenbach G. 1963. Hydroxamatkomplexe III. Eisen(III)-Austausch zwischen Sideraminen und Komplexonen. Diskussion der Bildungskonstanten der Hydroxamatkomplexe. Helv Chim Acta 46:1409–1422.
69. Nikaido H, Rosenberg EY. 1990. Cir and Fiu proteins in the outer membrane of Escherichia coli catalyze transport of monomeric catechols: study with beta-lactam antibiotics containing catechol and analogous groups. J Bacteriol 172:1361–1367.
70. Hall CM, Somprasong N, Hagen JP, Nottingham R, Sahl JW, Webb JR, Mayo M, Currie BJ, Podin Y, Wagner DM, Keim P, Schweizer HP. 2023. Exploring Cefiderocol Resistance Mechanisms in Burkholderia pseudomallei. Antimicrob Agents Chemother 67:e0017123.
71. Luscher A, Gasser V, Bumann D, Mislin GLA, Schalk IJ, Köhler T. 2022. Plant-Derived Catechols Are Substrates of TonB-Dependent Transporters and Sensitize Pseudomonas aeruginosa to Siderophore-Drug Conjugates. mBio 13:e01498-22.
72. Chatterjeet DK, Bourquin AW. 1987. Metabolism of Aromatic Compounds by Caulobacter crescentus. J Bacteriol 169:1993–1996.
73. Ely B. 1991. Genetics of Caulobacter crescentus, p. 372–384. *In* Bacterial Genetic Systems. Academic Press.
74. Hunter KA, Boyd PW. 2007. Iron-binding ligands and their role in the ocean biogeochemistry of iron. Environmental Chemistry 4:221.
75. Hassler CS, Schoemann V, Nichols CM, Butler EC V, Boyd PW. 2011. Saccharides enhance iron bioavailability to Southern Ocean phytoplankton. Proc Natl Acad Sci U S A 108:1076–81.
76. Buck KN, Lohan MC, Berger CJM, Bruland KW. 2007. Dissolved iron speciation in two distinct river plumes and an estuary: Implications for riverine iron supply. Limnol Oceanogr 52:843–855.
77. Cameron AJ, Liss PS. 1984. The stabilization of "dissolved" iron in freshwaters. Water Res 18:179–185.
78. Schwyn B, Neilands JB. 1987. Universal chemical assay for the detection and determination of siderophores. Anal Biochem 160:47–56.
79. Martin JD, Ito Y, Homann V V., Haygood MG, Butler A. 2006. Structure and membrane affinity of new amphiphilic siderophores produced by Ochrobactrum sp. SP18. Journal of Biological Inorganic Chemistry 11:633–641.
80. Moynié L, Luscher A, Rolo D, Pletzer D, Tortajada A, Weingart H, Braun Y, Page MGP, Naismith JH, Köhler T. 2017. Structure and Function of the PiuA and PirA Siderophore-Drug Receptors from Pseudomonas aeruginosa and Acinetobacter baumannii. Antimicrob Agents Chemother 61:10.1128/aac.02531-16.
81. Thanbichler M, Iniesta AA, Shapiro L. 2007. A comprehensive set of plasmids for vanillate- and xylose-inducible gene expression in Caulobacter crescentus. Nucleic Acids Res 35:e137–e137.
82. McLaughlin M, Hershey DM, Reyes Ruiz LM, Fiebig A, Crosson S. 2022. A cryptic transcription factor regulates Caulobacter adhesin development. PLoS Genet 18:e1010481.
83. Hyatt D, Chen GL, LoCascio PF, Land ML, Larimer FW, Hauser LJ. 2010. Prodigal: Prokaryotic gene recognition and translation initiation site identification. BMC Bioinformatics 11:119.
84. Tatusov RL, Galperin MY, Natale DA, Koonin E V. 2000. The COG database: a tool for genome-scale analysis of protein functions and evolution. Nucleic Acids Research 28: 33-36.
85. van Dongen Stijn and Abreu-Goodger C. 2012. Using MCL to Extract Clusters from Networks, p. 281–295. *In* van Helden Jacques and

Toussaint, A and TD (ed.), Bacterial Molecular Networks: Methods and Protocols. Springer New York, New York, NY.
86. Hartmann R, van Teeseling MCF, Thanbichler M, Drescher K. 2020. BacStalk: A comprehensive and interactive image analysis software tool for bacterial cell biology. Mol Microbiol 114:140–150.
87. Reyes Ruiz LM, Fiebig A, Crosson S. 2019. Regulation of bacterial surface attachment by a network of sensory transduction proteins. PLoS Genet 15:e1008022.
88. Shevchenko A, Wilm M, Vorm O, Mann M. 1996. Mass Spectrometric Sequencing of Proteins from Silver-Stained Polyacrylamide Gels. Anal Chem 68:850–858.
89. Sandy M, Butler A. 2009. Microbial iron acquisition: marine and terrestrial siderophores. Chem Rev 109:4580–95.

Acknowledgements

Research reported in this publication was supported in part by the National Institute of General Medical Science of the National Institutes of Health under award numbers R35GM131762 to S.C., P41GM135018 and R01GM038784 to T.V.O., and by Army Research Office contract W911NF2210105 to S.C.

Materials and Methods

Growth conditions and strain construction

C. crescentus strains were grown at 30˚C in one of several types of media as indicated. The peptone-yeast extract (PYE) medium (0.2% [w/v] peptone, 0.1% [w/v] yeast extract, 1 mM $MgSO_4$, 0.5 mM $CaCl_2$) is best described as a complex medium. In contrast M2X, is a defined medium based on M2 salt medium (6.1 mM Na_2HPO_4, 3.9 mM KH_2PO_4, 9.3 mM NH_4Cl, 0.25 mM $CaCl_2$, 0.5 mM $MgSO_4$, 10 μM Fe•EDTA chelate) that has 0.15% (w/v) xylose added as a carbon source. The Fe•EDTA chelate in M2X, and occasionally used to supplement PYE, is a 1:1 molar mix of $FeSO_4$ and EDTA (ferrous sulfate chelate solution kept at 4˚C, Sigma-Aldrich, F0518). However, the iron source in M2X was modified in some experiments, or omitted, as indicated. When ferric iron was used, a 100 mM $FeCl_3$ aqueous stock (pH ~2.0) kept at −20°C was thawed and used to make a working 10 mM stock that was added just before use to the final concentrations indicated. A 10 mM hemin stock solution was prepared in 1 M NaOH and diluted to the indicated final working concentrations. When an iron source (Fe•EDTA, $FeCl_3$, hemin) was added to solid medium, it was added after autoclaving. The water used for the preparation of all media was ultra-purified using a Barnsted GenPure water purification system (ThermoFisher). *E. coli* strains were grown at 37˚C in LB medium (1% [w/v] tryptone, 0.5% [w/v] yeast extract, 1% [w/v] NaCl). Growth media were solidified by the addition of 1.5% (w/v) agar when necessary. Antibiotics were used at the following concentrations in liquid and solid media as appropriate: *C. crescentus*, 5 μg/mL or 25 μg/mL kanamycin, 1 μg/mL or 2 μg/mL chloramphenicol, 1 μg/mL or 2 μg/ml tetracycline, 20 μg/mL nalidixic acid; *E. coli*, 50 μg/mL kanamycin, 20 μg/mL chloramphenicol, 10 μg/mL tetracycline.

Cells were also grown in environmental water samples from Lake Lansing and Northern Lake Huron (Hammond Bay). These samples were collected in high-density polyethylene analysis bottles provided by the Michigan Department of Environment, Great Lakes, and Energy (EGLE). Bottles were pre-rinsed with lake water from the sample site before sampling. Lake Huron waters were collected on November 10, 2023, in Presque Isle County, Michigan, USA, at 45°31′01.9″N 84°07′09.8″W. Lake Lansing waters were collected on February 14, 2024, from Ingham County, Michigan, USA, at 42°45′19.2″N 84°24′17.2″W. A quantitative elemental profile of these environmental samples was determined as described below.

Standard molecular biology techniques were used to construct all plasmids. Detailed information on strains, plasmids, and primers can be found in Table S6. To create plasmids for in-frame deletion allele replacements, the regions flanking the target gene were cloned into pNPTS138 (81). For the generation of fluorescent transcriptional reporter plasmids, promoter regions (400–500 bp upstream of the open reading frame) into the vector pPTM056 (82). For complementation, the entire coding sequences with their respective promoter regions were cloned into pMT603 (21), which integrates at the *xylX* locus.

All plasmids were individually introduced into the *C. crescentus* CB15 strain either by electroporation or by tri-parental mating. For allele replacements, a double recombination strategy was used to select merodiploid strains harboring each relevant pNPTS-based plasmid with kanamycin resistance, followed by *sacB* counterselection on PYE plates containing 3% (w/v) sucrose. PCR was used to evaluate colonies that were sucrose-resistant and kanamycin-sensitive to identify those colonies harboring the null allele. For the construction of strains with multiple gene deletions for TonB-dependent transporter genes, counterselection was performed on PYE sucrose plates supplemented with 10 μM Fe•EDTA (Sigma-Aldrich, F0518).

Tn-himar-seq to assess gene contributions to fitness in the presence of EDTA

An aliquot of a *C. crescentus* CB15 barcoded Tn-himar mutant library previously reported (39, 40) was grown in 5 mL of liquid PYE medium containing 5 μg/mL kanamycin for 8 h. One milliliter of this pre-culture was set aside as a reference, and four replicate cultures of 2 mL each in liquid PYE medium, alone or with 300 μM EDTA, were inoculated to a starting optical density at 660 nm (OD_{660}) of 0.01. The cultures were incubated in 100 mm × 14 mm glass culture tubes with shaking at 200 RPM at 30°C for 17 h, and 1 mL from each culture was collected by centrifugation for 3 min at 16,000*g*. The supernatants were discarded, and the cell pellets were resuspended in 10–20 μL of water and frozen at −20˚C.

Barcode abundances were determined following the method developed by Wetmore et al (29). Briefly, barcodes were amplified using Q5 polymerase (New England Biolabs) in a 20-μL reaction containing 1× Q5 reaction buffer, 1× GC enhancer, 0.8 units Q5 polymerase, 0.2 mM dNTPs, 0.5 μM of each primer, and 1 μL of the cell suspension, using the following amplification conditions: 98°C for 4 min, 25 cycles of (98°C for 30 sec, 55°C for 30 sec, and 72°C for 30 sec), 72°C for 5 min, followed by a hold at 4°C. The primer set consisted of a universal forward primer, Barseq_P1, and a uniquely indexed reverse primer, Barseq_P2_ITxxx, with the index number denoted by xxx (see ref (29)). The barcode amplification products were pooled and sequenced as 50-bp single-end reads on an Illumina MiSeq instrument, using Illumina TruSeq primers. Barcode sequence analysis was carried out using the fitness calculation protocol of Wetmore et al (29). Barcodes from each sample were counted and compiled using MultiCodes.pl and combineBarSeq.pl scripts (29). A barcode table was generated, from which the FEBA.R script was used to calculate fitness score relative to the reference starter culture.

Pangenome analysis

The genomes of 69 *Caulobacter* strains were analyzed using Anvi'o version 7.1 (60). The genomes incorporated into the analysis, as detailed in Table S2, were downloaded from the NCBI RefSeq database. These genomes were reformatted with the 'anvi-script-reformat-fasta' tool and integrated into an Anvi'o contigs database via 'anvi-gen-contigs-database'. Open reading frames (ORFs) were predicted using Prodigal (83). Predicted genes received functional annotations based on COG terms (84), and these annotations were subsequently appended to the contigs database. Gene clusters were delineated with the mcl algorithm (85), and a pangenome was constructed using 'anvi-pan-genome' with the parameters --mcl-inflation set to 6 and --min-occurrence set to 10.

Neighborhood analysis

The sequence of the CciO (encoded by gene locus CCNA_00027) protein was analyzed using the PSI-BLAST tool, set to default parameters, against the NCBI RefSeq database while excluding sequences from uncultured/environmental samples. Proteins that had greater than 95% query coverage and more than 65% identity were selected. The accession IDs of these proteins were submitted to the WebFLaGs server for neighborhood analysis, available at http://www.webflags.se/ (61). For brevity of presentation, a manually curated set of diverse loci is presented in Figure 2.

Serial dilution plating experiments

Overnight cultures grown in M2X medium with 10 μM $FeSO_4$•EDTA were centrifuged at 16,000*g* for 3 min at room temperature. Cell pellets were resuspended in iron-free liquid M2X medium to an OD_{660} of 0.2 and serially diluted 10-fold. Using a multichannel pipette, 5 μL from each dilution was spotted onto an agar plate. After the droplets were allowed to dry, the plates were incubated at 30°C for 2–3 days.

Growth measurements

A single colony from a strain grown on a PYE plate was inoculated into 2 mL of liquid PYE medium and grown overnight. The next day, the cultures were diluted to an OD_{660} of 0.15 and grown for 2 h before being used to

inoculate fresh cultures for the desired experimental condition (medium) at an OD_{660nm} of 0.01. Cultures were then incubated at 30°C with shaking at 200 rpm. After 16 h of growth, the optical density of the cultures was measured.

Measurement of growth in liquid M2X medium

Primary cultures in liquid M2X medium were inoculated from cells freshly grown on solid plates to an initial OD_{660} of 0.02–0.10 and grown overnight. These overnight cultures were diluted to an OD_{660} of 0.002 and allowed to grow for another day. The following morning, cells were collected by centrifugation and resuspended in iron-free liquid M2X medium. These cell suspensions were used to inoculate into various media at a starting OD_{660} of 0.01. Cultures were grown at 30°C with shaking at 200 rpm. Growth was periodically monitored by measuring OD_{660}. In conditions where iron was bound to a siderophore, $FeCl_3$ was combined with chelator in a 1:10 molar ratio prior to being added to the medium (see catecholate supplementation section below).

Cell size analysis

Wild-type and mutant *C. crescentus* cells were grown in PYE broth overnight. Starter cultures were used to inoculate 12 mL of PYE broth in 20 mL glass tubes at an OD_{660} of 0.01. Cultures were grown for 6 hours at 30˚C shaking at 200 RPM. To sample the cultures, 1 µl of cells were spotted on an agarose pad on a cover slide and imaged on a Leica DMI 6000 microscope in phase contrast with an HC PL APO 63x/1.4 numeric aperture (NA) oil Ph3 CS2 objective. Images were captured with an Orca-ER digital camera (Hamamatsu) controlled by Leica Application Suite X (Leica). Cell areas were measured from phase contrast images using BacStalk (86).

Transcriptome sequencing (RNA-seq)

The WT strain CB15 and the Δ*cciO* (lacking CCNA_00027) and Δ*cciT* (lacking CCNA_00028) mutant strains were grown overnight at 30 C in 2 mL of liquid M2X medium containing the standard 10 µM Fe•EDTA chelate concentration. These cultures were used to inoculate 10 mL of liquid M2X medium to a starting OD_{660} of 0.001 and then incubated overnight. After the OD_{660} exceeded 0.1, the cells were collected by centrifugation, rinsed with iron-free liquid M2X medium, and resuspended in 10 mL of liquid M2X medium containing 10 µM $FeCl_3$. The cell suspension was adjusted to an OD_{660} of 0.1 before being incubated at 30°C with shaking at 200 RPM for 2.5 h. Cells were harvested by centrifugation and stored at −80°C until RNA extraction. RNA was extracted using TRIzol (Invitrogen) as previously described (87). RNA-seq libraries were prepared utilizing an Illumina TruSeq Stranded RNA Kit and sequenced on an Illumina NextSeq 500 instrument at SeqCoast Genomics (Portsmouth, NH). The sequencing data were processed with the CLC Genomics Workbench 20 (Qiagen), aligning reads to the *C. crescentus* NA1000 genome (Genbank accession CP001340). RNA sequencing data are available in the NCBI GEO database under accession number GSE274268.

Analysis of transcription using fluorescent reporters

Strains harboring fluorescent transcriptional reporter plasmids to monitor the activity of the *feoB* or *cciT* promoters (fused to mNeonGreen) were cultured overnight in triplicate at 30°C in liquid PYE or M2X medium, each containing 1 µg/mL chloramphenicol. These cultures were diluted to an OD_{660} of 0.001 and incubated overnight at 30°C with shaking at 200 rpm. The next morning, these cultures were used to inoculate 500 µL of liquid medium in the wells of a clear 48-well plate. The plate lids were sealed onto the plate body with AeraSeal sealing film (RPI Research Products International) and incubated at 30°C with shaking at 155 RPM. After 1.5 or 2.5 h, OD_{660} and fluorescence (excitation at 497 ± 10 nm; emission at 523 ± 10 nm) were measured on a Tecan Spark 20M plate reader, and fluorescence values were normalized to the corresponding absorbance. Statistical analysis was conducted using GraphPad Prism version 10.1 or R.

Antibiotic/chemical sensitivity assays

To evaluate the susceptibility of *C. crescentus* strains to cefiderocol, streptonigrin, and CHIR-090, 200 µL of cell suspension adjusted to the same optical density (OD_{660} = 0.3) was spread onto the surface of PYE agar plates. For cefiderocol, an antibiotic gradient strip (Liofilchem MIC test strips) was placed centrally on each plate. For streptonigrin (Sigma-Aldrich) or CHIR-090 (Sigma-Aldrich), a 6-mm filter disc was loaded with 15 µL of 1 mg/mL streptonigrin or 2 mg/mL CHIR-090. The extent of sensitivity was determined by measuring the zone of inhibition.

Extraction of cell membrane proteins

Strains were grown overnight in 2 mL of PYE at 30˚C. The next day, these cultures were used to inoculate into 50 mL of PYE in the evening at an OD_{660} of 0.001. Once cultures reached an OD_{660} 0.4 they were induced with 100 µM dipyridyl and grown for 6 hours. Cultures were pelleted at 7197*g* for 10 minutes and the supernatants were removed. Pellets were then resuspended in 1 mL of ice-cold Tris pH 7.4 with 1 µL of DNAse and 1 µL of RNAse H. The resuspended cultures were lysed through sonication through 3-4 cycles of 20 second intervals with an amplitude of 20% and pulse of 1 second ON and 1 second OFF. Detergent based outer membrane protein extraction was accomplished as described in (67). For centrifugation steps during protein extraction, samples were spun at 20,000*g*.

SDS-PAGE separation of membrane fractions and protein mass spectrometry

Total protein concentration of 1.5 mg/mL was boiled in SDS sample buffer with 3% β-mercaptoethanol for 5 minutes. The samples were electrophoresed at room temperature in a 7.5% polyacrylamide gel. The gels were stained with Coomassie blue. Gels were destained with acetic acid solution and the bands containing the CciO protein were excised.

Gel bands were digested in-gel according to (88) with modifications. Briefly, gel bands were dehydrated using 100% acetonitrile and incubated with 10mM dithiothreitol in 100mM ammonium bicarbonate, pH~8, at 56C for 45min, dehydrated again and incubated in the dark with 50mM iodoacetamide in 100mM ammonium bicarbonate for 20min. Gel bands were then washed with ammonium bicarbonate and dehydrated again. Sequencing grade modified trypsin was prepared to 0.005ug/uL in 50mM ammonium bicarbonate and ~50uL of this was added to each gel band so that the gel was completely submerged. Bands were then incubated at 37C overnight. Peptides were extracted from the gel by water bath sonication in a solution of 60%Acetonitrile (ACN)/1%Trifluoroacetic acid (TFA) and vacuum dried to ~2uL. Peptides were then re-suspended in 2% ACN/0.1%TFA to 20uL. From this, 5uL were automatically injected by a Thermo (www.thermo.com) EASYnLC 1200 onto a Thermo Acclaim PepMap RSLC 0.1mm x 20mm c18 trapping column and washed for ~5min with buffer A. Bound peptides were then eluted onto a Thermo Acclaim PepMap RSLC 0.075mm x 500mm C18 analytical column over 35min with a gradient of 8%B to 40%B in 24min, ramping to 90%B at 25min and held at 90%B for the duration of the run (Buffer A = 99.9% Water/0.1% Formic Acid, Buffer B = 80% ACN/0.1% Formic Acid/19.9% Water). Column temperature was maintained at 50C using an integrated column heater (PRSO-V2, www.sonation.com).

Eluted peptides were sprayed into a ThermoFisher Q-Exactive HF-X mass spectrometer (www.thermo.com) using a FlexSpray spray ion source. Survey scans were taken in the Orbi trap (60000 resolution, determined at m/z 200) and the top 15 ions in each survey scan are then subjected to automatic higher energy collision induced dissociation (HCD) with fragment spectra acquired at 15000 resolution. The resulting MS/MS spectra were converted to peak lists using Mascot Distiller, v2.8.1 (www.matrixscience.com) and searched against all *C. crescentus* (*vibrioides*) protein entries available from Uniprot (downloaded from www.uniprot.org on 20201124), appended with common laboratory contaminants (downloaded from www.thegpm.org, cRAP project), using the Mascot searching algorithm, v 2.8.0.1. The Mascot output was then analyzed using Scaffold Q+S, v5.1.2 (www.proteomesoftware.com) to probabilistically validate protein identifications. Assignments validated using the Scaffold 1%FDR confidence filter are considered true.

Catecholate supplementation of growth media

A mixture of the iron and catecholate solutions was prepared in a 1:10 molar ratio such that the catecholate was 10-fold more abundant than $FeCl_3$. This mix was added to M2X medium as the sole iron source to reach a concentration of 1 µM $FeCl_3$ and 10 µM catecholate (2,3-dihydroxybenzoic acid, 3,4-dihydroxybenzoic acid, or chlorogenic acid). Once the medium was prepared, it was immediately used for inoculation as described above for a growth curve.

Cation supplementation in PYE medium containing 300 µM EDTA

To evaluate the effects of cation supplementation on growth in liquid PYE medium containing 300 µM EDTA, the reagents were mixed in the following manner. First, appropriate volumes of EDTA and cation stock solutions were deposited on the opposite sides of a 50-mL tube. Then, liquid PYE medium was added to the tube and shaken. The mixture was dispensed in 2-

mL aliquots into glass culture tubes and inoculated as described above for 16-h growth experiments.

Cultivation of *C. crescentus* in lake water

A colony from the WT, Δ*cciO*, or Δ*cciT* strain grown on PYE agar plates was inoculated into liquid PYE medium and grown overnight. The next morning, cells were collected by centrifugation and washed three times with 0.2 μM filtered lake water (collected as described above) by serially pelleting and resuspending the cells. After the last wash, the resuspended cells were used to inoculate filtered lake water at a starting OD_{660} of 0.2 and serially diluted 10-fold three times (for a factor of 10^3). Then 100 μL of the final dilution was used to inoculate 10 mL of desired lake water. Culture density was assessed then and after 5, 10, 24, and 29 h of growth by determining the number of colony-forming units.

Measurement of total organic carbon, nitrogen, and sulfate contents of environmental water samples

Lake Lansing and Lake Huron water samples were submitted to EGLE for content analysis of total organic carbon (TOC), nitrogen, sulfate, chloride, conductivity, and alkalinity. TOC content was measured following the persulfate oxidation method 5310C (ASTM Standards). Nitrogen content was measured following the Total Kjeldahl Nitrogen by Semi-Automated Colorimetry approach (EPA method 351.2). Sulfate ion content was measured following the standard test method for sulfate ion in water (ASTM method D516-16). Additional lake analytical methods are provided in Table S5.

Inductively coupled plasma mass spectrometry (ICP-MS) analysis

All blanks, calibration standards, and ICP-MS samples were prepared using trace-metal-grade nitric acid (70% [w/v], Fisher Chemical, Cat. No. A509P212), ultrapure water (18.2 MΩ·cm at 25°C, Millipore Sigma Milli-Q® IQ7000 Ultrapure Water Purification System), and metal-free polypropylene conical tubes (15 mL and 50 mL, Labcon, Petaluma, CA, USA). Cellular phosphorus and iron contents of *C. crescentus* WT and mutant strains were measured by ICP-MS. Harvested bacterial cultures were spin-washed with Milli-Q water with or without 10 micromolar EDTA in the metal-free conical tubes. The bacterial cell pellets were dried in a heating block at 80ºC overnight prior to extraction. For liquid samples such as a medium or lake water samples, 100–500 μL of each sample was also dried in the heating block or oven at 80ºC overnight with the conical tube caps loosened. Dried cell pellets and liquid residues were digested in 150 μL of 70% (w/v) nitric acid at 70ºC for 3–4 h or until the pellet was dissolved completely. Following digestion, the final volume of each ICP-MS sample was brought up to 5 mL with Milli-Q water to yield a 3% (w/v) nitric acid matrix. The elemental concentration of all digested samples and calibration standards were determined on a parts per billion (ppb, μg/L) scale using an Agilent 8900 Triple Quadrupole ICP-MS (Agilent, Santa Clara, CA, USA) equipped with an Agilent SPS 4 Autosampler, integrated sample introduction system (ISIS), x-lens, and micromist nebulizer. Daily tuning of the instrument was accomplished using a tuning solution (Agilent, Cat. No. 5185-5959) containing Li, Co, Y, Ce, and Tl. Global tune optimization was based on optimizing intensities for ^{7}Li, ^{89}Y, and ^{205}Tl while minimizing oxides ($^{140}Ce^{16}O/^{140}Ce < 1.5\%$) and doubly charged species ($^{140}Ce^{++}/^{140}Ce^{+} < 2\%$). Following global instrument tuning, gas mode tuning in He KED and O_2 mode was accomplished using the same tuning solution. In KED mode (using 100% ultra-high-purity [UHP] He, Airgas), intensities for ^{59}Co, ^{89}Y, and ^{205}Tl were maximized while minimizing oxides ($^{140}Ce^{16}O/^{140}Ce < 0.5\%$) and doubly charged species ($^{140}Ce^{++}/^{140}Ce^{+} < 1.5\%$) with short-term relative standard deviations (RSDs) < 3.5%. In O_2 mode (using 100% UHP O_2, Airgas) intensities for ^{59}Co, ^{89}Y, and ^{205}Tl were maximized with short-term RSDs < 3.5%. Internal standardization was accomplished inline using the ISIS valve and a 200-ppb internal standard solution prepared in 3% (w/v) trace nitric acid in ultrapure water consisting of Bi, In, ^{6}Li, Sc, Tb, and Y (IV-ICPMS-71D, Inorganic Ventures).

The isotopes selected for analysis of media samples were ^{31}P ($^{31}P^{16}O$), ^{56}Fe, ^{57}Fe, ^{58}Ni, ^{59}Co, ^{60}Ni, ^{63}Cu, ^{64}Zn, ^{65}Cu, ^{66}Zn, ^{75}As, ^{78}Se ($^{78}Se^{16}O$), ^{95}Mo, ^{80}Se ($^{80}Se^{16}O$), and ^{111}Cd with ^{6}Li, ^{45}Sc, and ^{89}Y used for internal standardization. For ICP-MS calibration standard preparation, a 10-ppm stock solution containing As, Ca, Cd, Co, Cr, Cu, Fe, Gd, K, Mg, Mn, Mo, Na, Ni, P, Pt, S, Se, V, and Zn (IV-65024, Inorganic Ventures, Christiansburg, VA, USA) was diluted with 3% (w/v) trace nitric acid in ultrapure water to a final element concentration that covers a range of 0.02–800 ppb. Element concentrations in each sample were derived from a calibration curve generated by Mass Hunter software (Agilent).

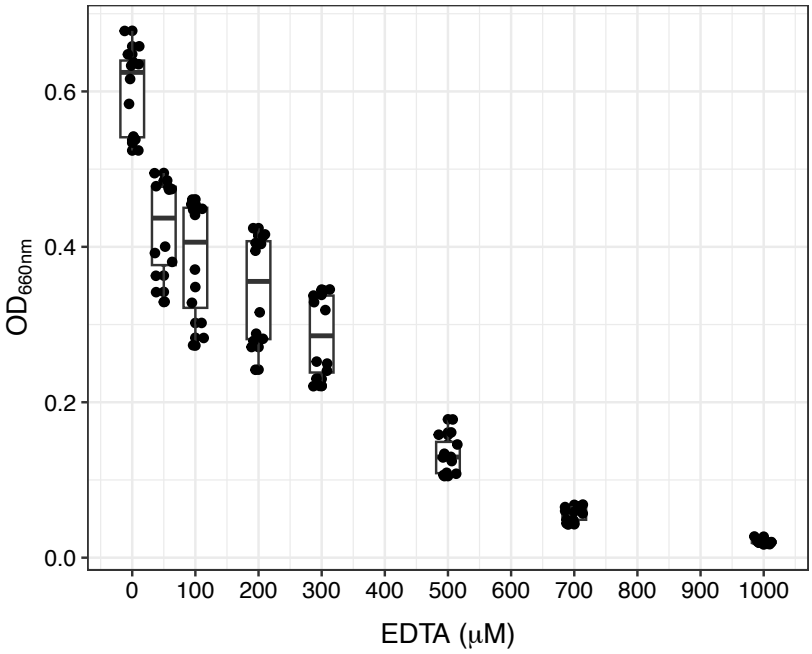

Figure S1. EDTA attenuates growth of *C. crescentus* in a dose-dependent manner. Optical density at 660 nm of cultures of *C. crescentus* strain CB15 after 16 h of cultivation in complex liquid medium (PYE) with increasing concentrations of EDTA. All cultures were inoculated at an initial OD_{660} of 0.01. Data represent 12 biological replicates. In the boxplots, the midline represents the median, and the edges of the box represent the 25th and 75th percentiles. Individual data points are shown as black circles.

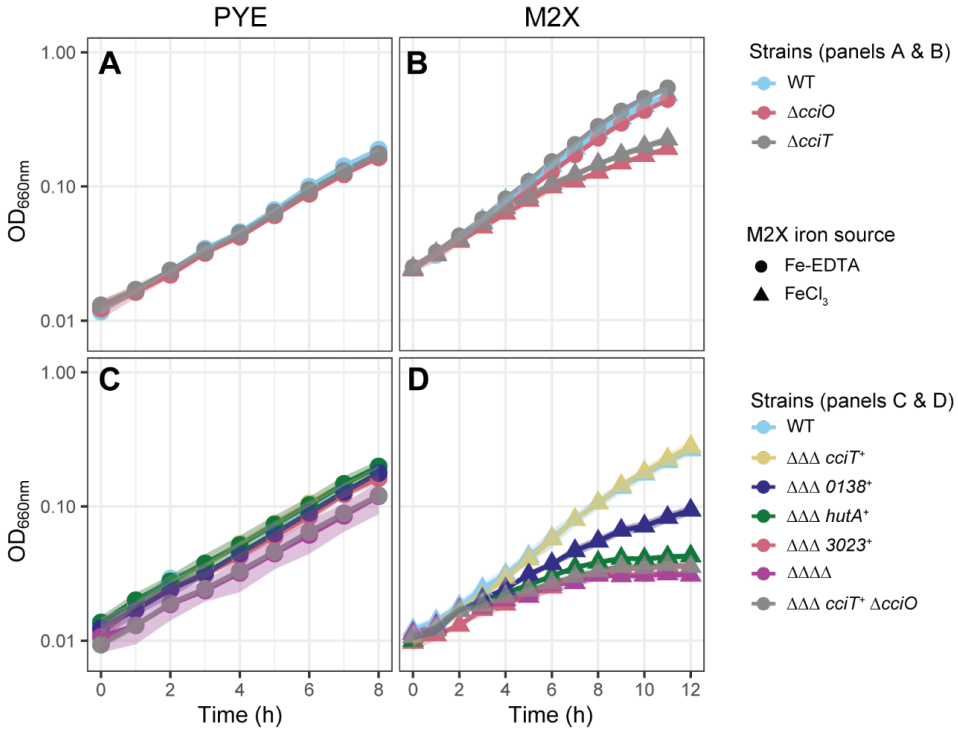

Figure S2. Growth of *cciT* and *cciO* mutants in complex (PYE) and defined (M2X) media. (A&C) Growth of strains measured by optical density at 660 nm (OD_{660}) in complex liquid PYE medium without iron supplementation. **(B&D)** Growth of strains in defined liquid M2X medium where the sole iron source is either 10 μM Fe•EDTA (circles) or 10 μM $FeCl_3$ (triangles). **A&B** show growth of the WT, Δ*cciO*, and Δ*cciT* mutant strains. **C&D** show growth of strains retaining only one of the four Fur-regulated TBDT genes, a strain lacking all four Fur-regulated TBDT genes (ΔΔΔΔ), and a strain in which *cciT* is the only Fur-regulated TBDT gene and *cciO* has been deleted (*cciT*+ ΔΔΔ Δ*cciO*). Values are means ± SD (as shaded areas) from three biological replicates generated on the same day. The SD is too small to be visible in most cases.

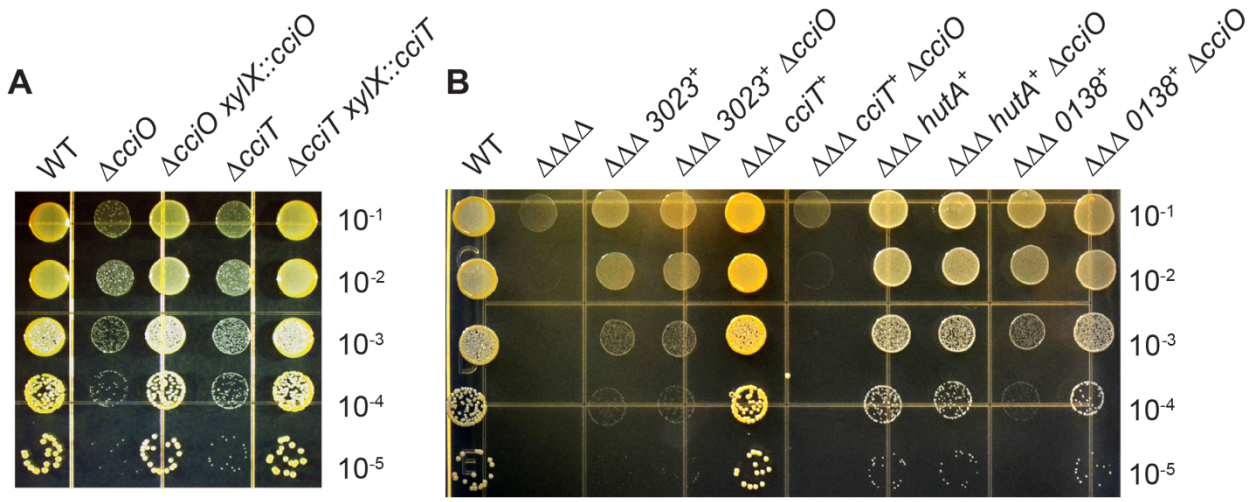

Figure S3. *cciO* is specifically required for *cciT* to support *C. crescentus* growth on solid medium. (A) Serial dilutions (10-fold) of WT, Δ*cciO* and Δ*cciT* mutants, and genetically complemented strains expressing *cciO* or *cciT* from the *xylX* chromosomal locus. **(B)** Serial dilutions of WT and mutant strains retaining only one of the four Fur-regulated TBDT genes (*cciT*, CCNA_00138, CCNA_03023, and *hutA*) in a background encoding or lacking *cciO* (Δ*cciO*). Strains were spotted onto solid complex medium (PYE). Dilution factor is indicated on the right.

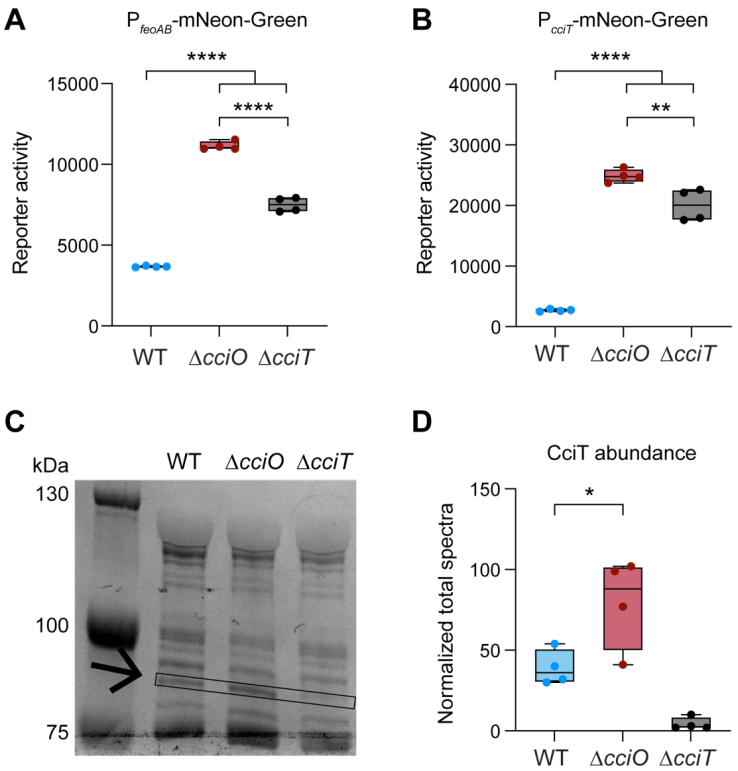

Figure S4. Transcription reporter and protein mass spectrometry validation of differences in Fur-dependent gene expression in the *cciT* and *cciO* deletion strains. Fluorescence signal from promoter:mNeonGreen transcriptional reporter cassettes with **(A)** the Fur-regulated *feoAB* promoter (P_{feoAB}) or **(B)** the Fur-regulated *cciT* promoter (P_{cciT}) in WT, Δ*cciT*, and Δ*cciO* strains grown in the same conditions as in the RNA-seq experiment (M2X defined medium with $FeCl_3$; see Figure 4). **(C)** SDS-PAGE gel of outer membrane protein preparations from WT, Δ*cciT*, and Δ*cciO* strains cultivated in liquid PYE medium containing 100 µM of the intracellular iron chelator dipyridyl. Membrane proteins were extracted as described (67). The band corresponding to the size of CciT is marked with a box and arrow on the Coomassie brilliant blue-stained gel. **(D)** Mass spectrometry quantification of CciT tryptic peptides isolated from gel slices cut from the marked box in panel C. Peptides were quantified from four independent outer-membrane protein preparations. The significance of differences in transcription or tryptic peptide levels was determined by one-way ANOVA followed by Tukey's post-hoc test for each pairwise comparison except in D, where we only compared CciT levels in WT and Δ*cciO* because the transport protein is not produced in Δ*cciT* (* $p < 0.05$; ** $p < 0.01$; **** $p < 0.00001$).

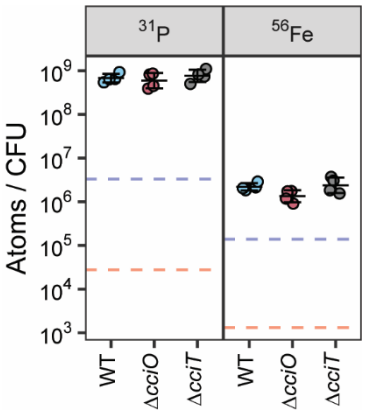

Figure S5. ICP-QQQ-MS elemental analysis of WT, *ΔcciO*, and *ΔcciT* strains of *C. crescentus* cultivated in peptone-yeast extract (PYE) complex medium. Phosphorus (P) and iron (Fe) concentrations for each replicate normalized to the number of colony-forming units. The dashed blue line represents the background equivalent concentration (BEC) of the element in the digestion blanks. The dashed orange line represents the detection limit (DL) of the element. The data points shown have been corrected for BEC during the calibration process. The BEC and DL lines are provided to demonstrate the instrument's detection capability and the background matrix concentration.

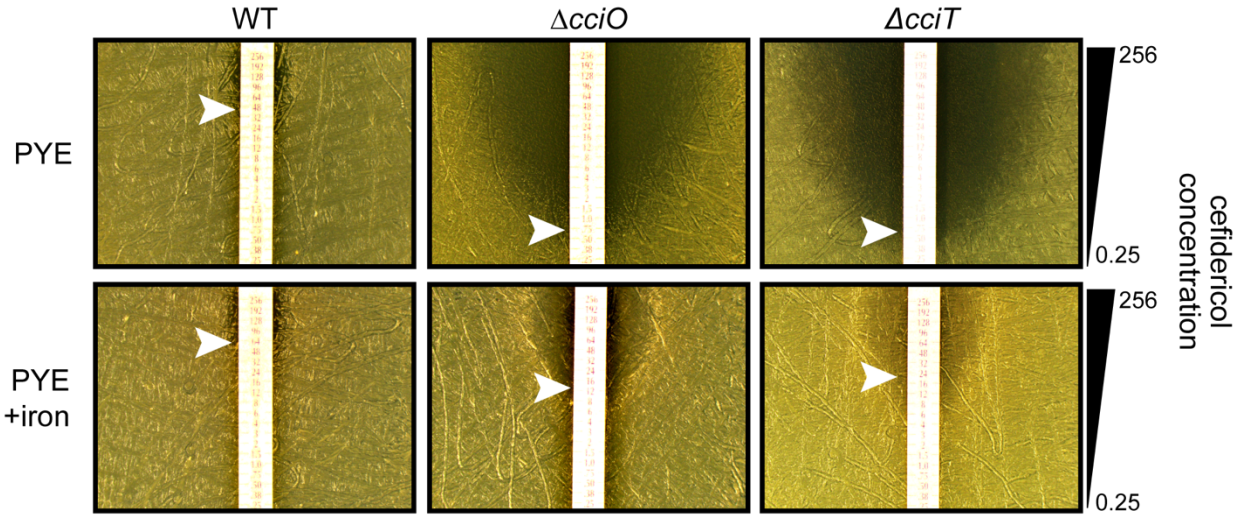

Figure S6. Sensitivity of *C. crescentus* wild-type and strains lacking *cciO* or *cciT* to the catechol-cephalosporin "Trojan horse" antibiotic, cefiderocol. Tests were conducted on complex (PYE) medium without (top) and with (bottom) supplementation of the growth medium with 10 μM Fe•EDTA. Arrowheads indicate approximate minimal inhibitory concentration in each condition. The range of cefiderocol concentration in the strip is indicated on the right.

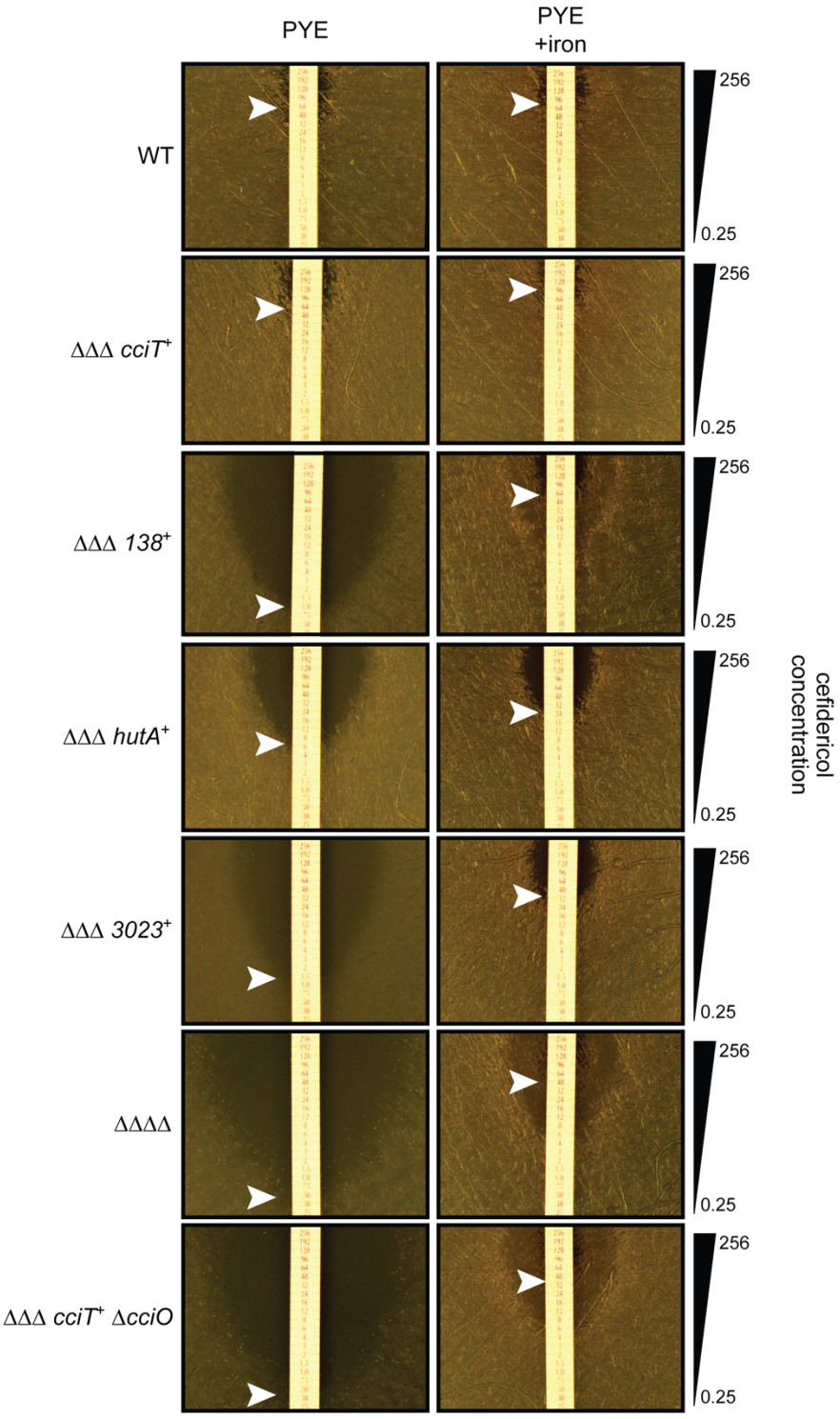

Figure S7. Wild-type *C. crescentus* and a strain expressing *cciT* but lacking the other three Fur-regulated TBDT genes (*cciT*+ ΔΔΔ) are resistant to cefiderocol. Any strain lacking *cciO or cciT* is sensitized to cefiderocol. Addition of 10 μM Fe•EDTA to the medium both improved growth and conferred some cefiderocol resistance compared to that in PYE medium alone. The range of cefiderocol concentration in the strip is indicated on the right. Minimal inhibitory concentration is marked with a white arrow.

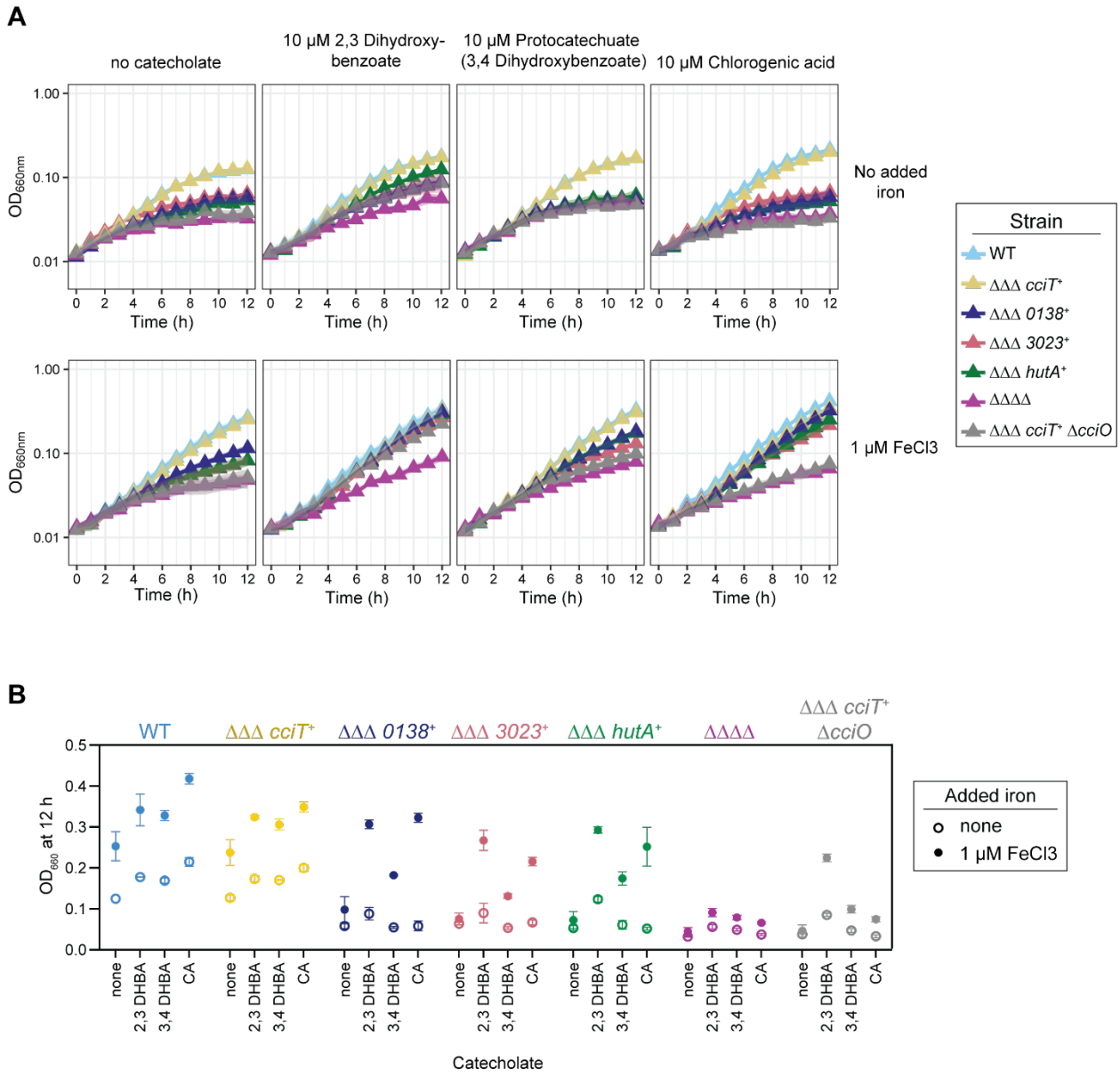

Figure S8. Effects of catecholates and iron on growth in defined medium. (A) Growth curves of strains grown in defined liquid M2X-based medium with no added iron (top) or with the addition of 1 μM $FeCl_3$ (bottom), in the presence of 10 μM of three different catecholates (labeled above). **(B)** Optical densities at 600 nm of cultures after 12 h of growth, extracted from the curves in A.

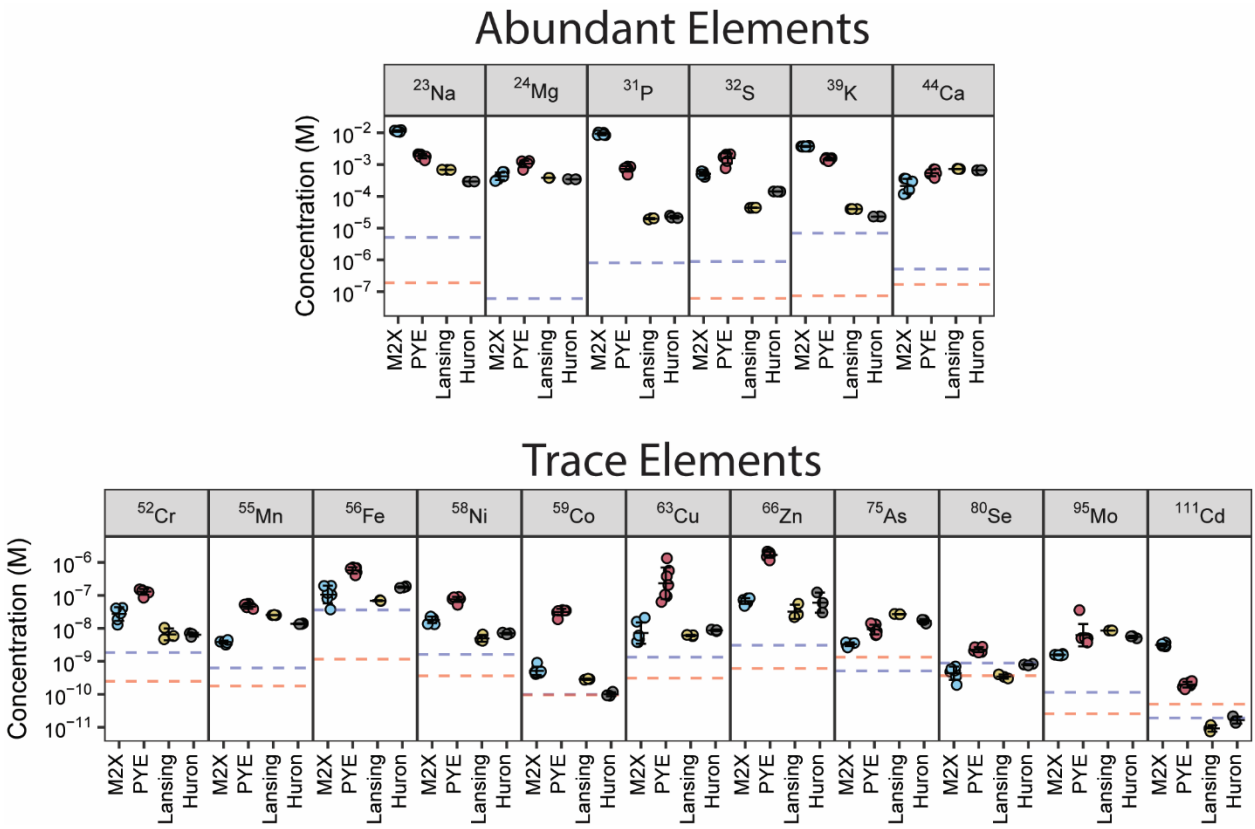

Figure S9 ICP-QQQ-MS elemental analysis of growth media. Quantitative elemental profiles of liquid M2X medium (without added iron supplement), liquid PYE medium, and water collected from Hammond Bay in Lake Huron (collected November 2023) and Lake Lansing public dock at South Lake Lansing Park (collected February 2024), measured by ICP-MS-QQQ. Data represent nine independent measurements for each condition (3 independent samples measured 3 times). Mean ± SD are overlayed with the individual data points. The laboratory media were prepared three times and measured in technical triplicates. The lake sources were each measured on one sampling day where three samples were prepared and measured in technical triplicate. The dashed blue line represents the background equivalent concentration (BEC) of the element in the digestion blanks. The dashed orange line represents the detection limit (DL) of the element. The data points shown have been corrected for BEC during the calibration process. The BEC and DL lines are provided to demonstrate the instrument's detection capability and the background matrix concentration.

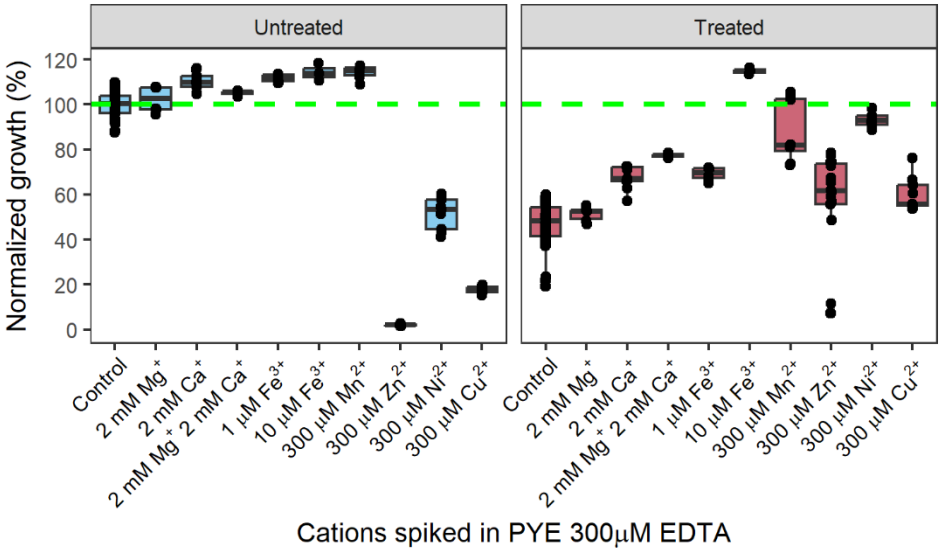

Figure S10. Rescue of EDTA-dependent growth inhibition by select cations. Density of *C. crescentus* cultures after 16 h of growth of was measured spectrophotometrically (OD_{660}) in the presence of indicated cations, without (Untreated) or with (Treated) 300 μM EDTA. Values were normalized to WT growth in untreated (Control) PYE medium. For each condition, at least three biological replicates were measured. Summary box plots representing the median, 25th and 75th percentiles are overlayed with the individual data points.